

Quantum-interference-induced pairing in antiferromagnetic bosonic t - J model

Hao-Kai Zhang,¹ Jia-Xin Zhang,^{2,3,1,*} Ji-Si Xu,¹ and Zheng-Yu Weng¹

¹*Institute for Advanced Study, Tsinghua University, Beijing 100084, China*

²*French American Center for Theoretical Science, CNRS,*

KITP, Santa Barbara, California 93106-4030, USA

³*Kavli Institute for Theoretical Physics, University of California, Santa Barbara, California 93106-4030, USA*

(Dated: September 25, 2024)

The pairing mechanism in an antiferromagnetic (AFM) bosonic t - J model is investigated via large-scale density matrix renormalization group calculations. In contrast to the competing orders in the fermionic t - J model, we discover that a pair density wave (PDW) of tightly bound hole pairs coexists with the AFM order forming a “supersolid” at small doping in the bosonic model. The pairing order collapses at larger doping to a superfluid of single-boson condensation with the spin background polarized to a ferromagnetic (FM) order simultaneously. This pairing phase will disappear once a hidden quantum many-body Berry phase in the model is artificially switched off. Such a Berry phase, termed the phase string, introduces the sole “sign problem” in this bosonic model and imposes quantum phase frustration in the interference pattern between spin and charge degrees of freedom. Only via tightly pairing of doped holes, can such quantum frustration be most effectively erased in an AFM background. By contrast, the pairing vanishes as such a Berry phase trivializes in an FM background or is switched off by a sign-problem-free model (the Bose-Hubbard model at large U). The pairing mechanism proposed here is inherently quantum and many-body, stemming from exotic interference patterns caused by strong correlation effects, which is distinct from the semi-classical mechanisms based on bosonic fluctuations. Experimental schemes have been recently proposed to realize the bosonic t - J model on ultracold Rydberg atom arrays, offering a useful platform to test the present unconventional pairing mechanism, which is also relevant to the fermionic case associated with high-temperature superconductors.

The pairing mechanism of unconventional superconductivity (SC) from doping antiferromagnetic (AFM) Mott insulators is one of the central puzzles in modern condensed matter physics [1–3]. The two-dimensional Hubbard model and the related t - J model are believed to capture many of the essential aspects of such systems [4–8]. Despite intensive efforts and considerable progress over the past decades in analytical and numerical studies [3, 7–31], an undisputed systematic understanding of their ground and thermal states remains elusive due to the inherent complexity of them as paradigmatic models of strongly correlated systems.

In recent years, quantum simulators especially ultracold atoms have brought new opportunities for exploring unconventional SC mechanisms [32–42] and other strongly correlated quantum matter [43–53]. These simulators can reach regimes that are numerically difficult to access and are flexible in tuning and probing microscopic correlations. The Hubbard model and effectively the t - J model can be artificially realized by cooling and trapping fermionic atoms such as ^6Li into optical lattices [32–46]. The lowest temperatures reached in such realizations are about half of the superexchange energy scale, where extended-range AFM correlations have been observed [35] yet the potential SC phase still requires further lower temperatures.

On the other hand, various quantum spin (equivalently hard-core boson) models have been recently realized on

Rydberg atom arrays [47–53], where the spin or boson states are encoded into the internal states of atoms such as ^{87}Rb . Programmable quantum gates have been implemented [54, 55] enabling measurements beyond diagonal density correlations. Experimental schemes have been recently proposed to realize the AFM bosonic t - J model on such platforms [56]. This model still describes doped Heisenberg antiferromagnets but with bosonic dopants. Comparative studies of the bosonic and fermionic t - J models, alongside advanced cold atom simulations, are promising to offer deeper insights into the physics of doped Mott insulators.

In this article, we identify the critical role of quantum frustration in the doped bosonic t - J model as a decisive factor that determines the emergence of a non-trivial pairing order on the AFM spin background. By performing large-scale density-matrix renormalization group (DMRG) simulations, we establish a ground-state phase diagram [cf. Fig. 1(a)] for the AFM bosonic t - J model on a 2D square lattice with varying doping levels. Upon doping the isotropic Heisenberg antiferromagnet in long-range AFM order, a robust spin-singlet pairing order emerges with a pair density wave (PDW) at momentum (π, π) , which coexists with the AFM order symbiotically resembling the feature of supersolids. The boson pairs are tightly bound in space and exhibit p -wave symmetry up to the PDW oscillation. Importantly, the single-particle propagation is strongly suppressed in this PDW phase, prohibiting the Bose-Einstein condensation (BEC) that occurs in common interacting bosonic systems. Only after exceeding a critical doping level, does the ground state turn into a conventional superfluid (SF) with the spin

* jiaxin_zhang@ucsb.edu

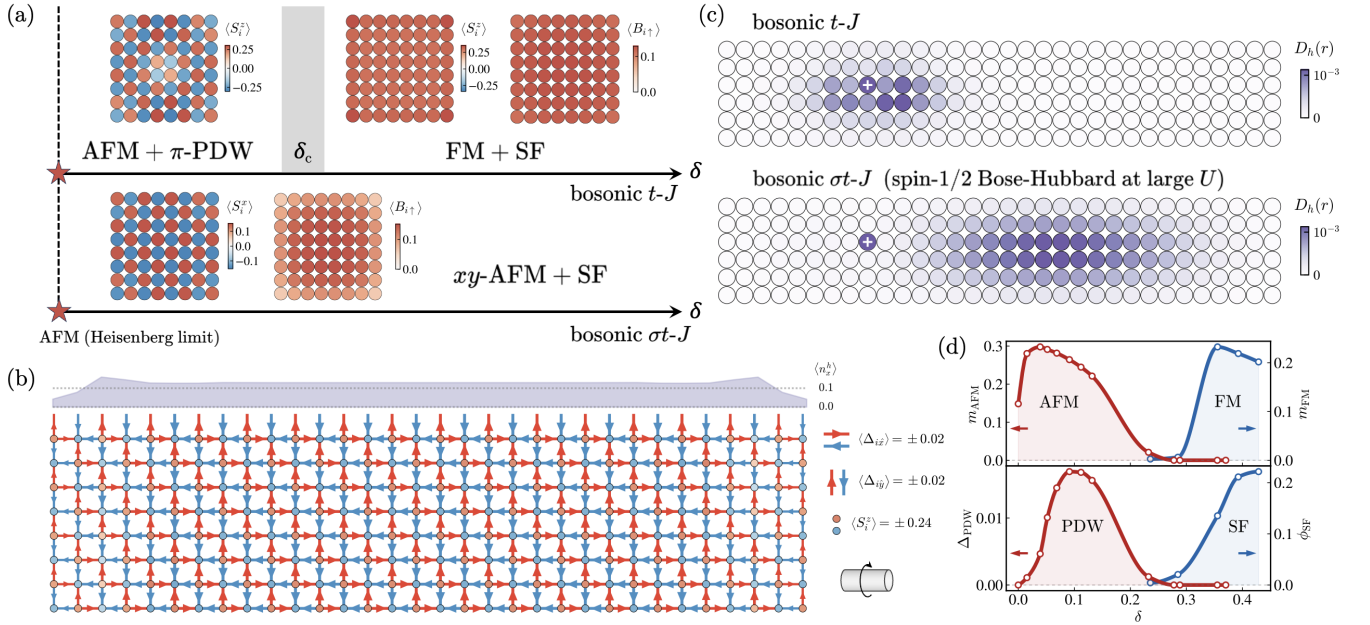


FIG. 1. (a) The ground state phase diagram of the 2D bosonic t - J model and σt - J model at $t/J = 3$ and varying hole doping δ determined by simulation results on width-4, 6, 8 square lattices. At half-filling, both models are reduced to the Heisenberg model. Upon doping, the former model enters a pair density wave (PDW) phase on an antiferromagnetic (AFM) spin background and then goes into a ferromagnetic (FM) superfluid (SF) phase after $\delta_c \approx 0.2$. By contrast, the latter model directly enters an SF phase with an easy-plane AFM order. Representative local order parameters on 8×8 lattices are shown accordingly. (b) A representative PDW pattern on a 32×8 cylinder. The corresponding AFM order and the hole density profile are also shown. The width of the arrows is proportional to the magnitude of the spin-singlet pairing order $\langle \Delta_{i\alpha} \rangle$. The arrows indicate the fact that bosonic singlets are directed, in contrast to undirected fermionic singlets. (c) The hole-hole correlation $D_h(r)$ for the two models with two doped holes. The cross represents the reference site. (d) The magnitudes of global order parameters as functions of doping levels on a 32×8 cylinder.

background being polarized into a Nagaoka ferromagnet (FM) concomitantly.

Namely, we find a robust phase in the low-doping regime where the doped holes can propagate coherently on the AFM spin background only if they are tightly bound in pairs. This pairing can be well understood by the intrinsic quantum frustration in the model, where the hopping of a doped hole can accumulate a \mathbb{Z}_2 Berry phase determined by the orientation of the spin exchanged with the hole at each hopping step. Such a Berry phase will result in destructive interference for the single-hole motion, whereas by canceling the \mathbb{Z}_2 phases, the tightly bound pairs can realize a constructive coherent propagation. If such frustration is artificially removed, the pairing order will disappear and be replaced by a conventional SF. Finally, we discuss the analogy to the flat-band SC, the implication to the fermionic case, and the potential experimental observations in cold atom simulations.

Results

Model and phase diagram

We first present the numerical results in full and then discuss the physical interpretation. We consider the spin-1/2 hard-core bosonic t - J model on a 2D square lattice of size $N = L_x \times L_y$. The Hamiltonian reads $H_{t-J} = \mathcal{P}_s(H_t + H_J)\mathcal{P}_s$ composed of a hopping term and

an isotropic AFM spin-exchange term, i.e.,

$$H_t = -t \sum_{\langle ij \rangle \sigma} (B_{i\sigma}^\dagger B_{j\sigma} + \text{H.c.}),$$

$$H_J = J \sum_{\langle ij \rangle} \left(\mathbf{S}_i \cdot \mathbf{S}_j - \frac{1}{4} n_i n_j \right).$$
(1)

Here $B_{i\sigma}^\dagger$ and $B_{i\sigma}$ are the creation and annihilation operators of a hard-core boson of spin $\sigma \in \{\uparrow, \downarrow\}$ at site $i = (x, y)$. \mathbf{S}_i and $n_i = \sum_{\sigma} n_{i\sigma}$ are the spin and particle number operator. $\langle ij \rangle$ denotes nearest-neighbor (NN) links. The Hilbert space is restricted by the no-double occupancy constraint $n_i \leq 1$ via the projector \mathcal{P}_s . We set $J = 1$ as the energy unit with $t/J = 3$ and vary the hole doping level $\delta = \sum_i \langle n_i^h \rangle / N$ where $n_i^h = 1 - n_i$. We implement DMRG simulations using both grand canonical ensembles (GCE) [26, 27] and canonical ensembles (CE) [17–25] independently to obtain reliable results. See Methods for the numerical details [57].

The long-range AFM order at half-filling persists to the finite-doping regime until a critical doping $\delta_c \approx 0.2$, as evidenced by the spontaneous broken local magnetization $\langle S_i^z \rangle$ in Néel order from GCE simulations in Fig. 1(a), and the quasi-long-range spin-spin correlations $F_\gamma(r) = \langle S_{i_0}^\gamma S_{i_0+r}^\gamma \rangle$ from CE simulations in Figs. 2(c) and

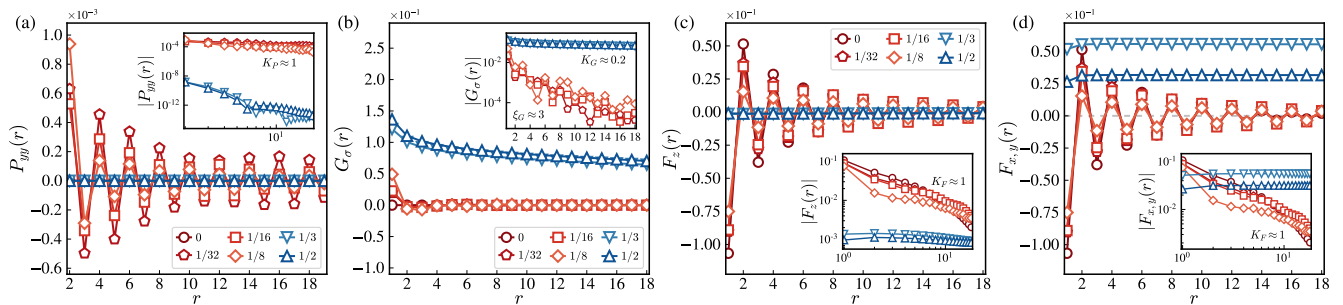


FIG. 2. Correlation functions in the ground state of the bosonic t - J model on cylinders of size 32×4 or 36×4 with $t/J = 3$ and varying doping level δ labeled by different markers. (a) The spin-singlet pair-pair correlation. (b) The single-particle Green's function. (c) and (d) The spin-spin correlation along the S^z and $S^{x,y}$ directions. The inset shows the logarithmic or semi-logarithmic plot with the fitted power exponent K or correlation length ξ . The red and blue markers indicate the AFM-PDW and FM-SF phases, respectively.

(d). Here $\gamma \in \{x, y, z\}$ denotes the spin component and $i_0 = (x_0, y_0)$ with $x_0 = L_x/4$ denotes the reference site. The doped holes even enhance the AFM order as evidenced by the slower decay of $F_\gamma(r)$ at finite doping and the larger order parameter $m_{\text{AFM}} = \sum_i (-1)^{x+y} \langle S_i^z \rangle / N$ in Fig. 1(d).

A robust singlet pairing order $\langle \Delta_{i\alpha} \rangle$ emerges upon doping with the sign staggered in both spatial directions, giving rise to a PDW order [58–61] at momentum (π, π) , coexisting with the AFM order, as shown by the spatial pattern in Fig. 1(c) and the order parameter $\Delta_{\text{PDW}} = \sum_{i\alpha} (-1)^{x+y} \langle \Delta_{i\alpha} \rangle / (2N - L_y)$ in Fig. 1(d). Here $\Delta_{i\alpha} = \frac{1}{\sqrt{2}} \sum_{\sigma} \sigma B_{i,\sigma} B_{i+\alpha, -\sigma}$ is the spin-singlet pair operator. $\alpha \in \{\hat{x}, \hat{y}\}$ is the NN link and the coefficient σ takes $\{+1, -1\}$ for $\{\uparrow, \downarrow\}$. The PDW is also observed by the quasi-long-range pair-pair correlation $P_{\alpha\beta}(r) = \langle \Delta_{i_0\alpha}^\dagger \Delta_{(i_0+r),\beta} \rangle$ with staggered oscillations in Fig. 2(a). Importantly, the single-particle Green's function $G_\sigma(r) = \langle B_{i_0,\sigma}^\dagger B_{(i_0+r),\sigma} \rangle$ decays exponentially, as shown in Fig. 2(b), which indicates that $\langle \Delta_{i\alpha} \rangle$ is a primary pairing order instead of a secondary result from a single-boson condensation.

The tight binding of hole pairs also manifests in the hole-hole correlation $D_h(r) = \langle n_{i_0}^h n_{(i_0+r)}^h \rangle$ in a two-hole-doped system, as shown in Fig. 1(c). It decays exponentially with a correlation length of about one lattice constant, implying an extremely small pair size. Moreover, the hole density distribution tends to be uniform in the bulks at moderately low doping, as shown by the profile $\langle n_x^h \rangle = \sum_y \langle n_{x,y}^h \rangle / L_y$ in Fig. 1(b), compared to the distinct charge and spin stripes observed in the fermionic case that compete with the SC order [15–27].

The pairing and AFM orders break down simultaneously if the doping level exceeds a critical point (or region), and are replaced by a single-particle condensation as in common interesting boson systems. This is evidenced by the prominent order parameter $\langle B_{i\sigma} \rangle$ in Fig. 1(a) and the extremely slow decay of $G_\sigma(r)$ in Fig. 2(b). Compatible with the single-particle's unimpeded motion, the spin background is polarized to an FM

order like the Nagaoka ferromagnetism [6], as indicated by $\langle S_i^z \rangle$ in Fig. 1(a) and $F_\gamma(r)$ in Figs. 2(c) and (d), respectively. This phase transition can be seen clearly from the evolution of order parameters with the doping level in Fig. 1(d). $m_{\text{FM}} = \sum_i \langle S_i^z \rangle / N$ and $\phi_{\text{SF}} = \sum_{i\sigma} \langle B_{i\sigma} \rangle / N$ represent the FM and SF order parameters, respectively.

Quantum frustration from an exact Berry phase

The usual fate for bosons at low temperatures is BEC, once the single-particle phase coherence is established throughout the system. For example, the Bose-Hubbard model at fractional filling exhibits a superfluid phase all the time [62, 63]. A significant feature of the bosonic t - J model revealed by our simulations is the absence of a single-boson BEC phase in the low doping regime at zero temperature. Instead, a robust pairing order emerges as shown in Fig. 1(a). This suggests that the bosonic t - J model may possess some hidden intrinsic phase frustration for the single-boson motion.

To clarify this point, we first consider an undoped Mott insulator described by the Heisenberg model H_J on a square lattice. We know H_J is stochastic under the Marshall basis [6], i.e., all the non-zero matrix elements of $(-H_J)$ are positive after performing a gauge transformation that attaches a negative sign for all the \downarrow spins on sublattice A (see Methods)

$$|\downarrow\rangle_A \rightarrow -|\downarrow\rangle_A. \quad (2)$$

Hence the Heisenberg model on a bipartite lattice is sign-problem-free. However, upon doping, the hopping of doped holes will disorder the above Marshall sign rule. A nontrivial sign structure τ_C will then explicitly appear in the partition function

$$Z_{t-J} \equiv \text{Tr} e^{-\beta H_{t-J}} = \sum_C \tau_C W_{t-J}[C], \quad (3)$$

where $W_{t-J}[C] \geq 0$ is the non-negative weight corresponding to each closed imaginary-time evolution path C . The phase factor τ_C has the following exact form

$$\tau_C = (-1)^{N_\downarrow^h}, \quad (4)$$

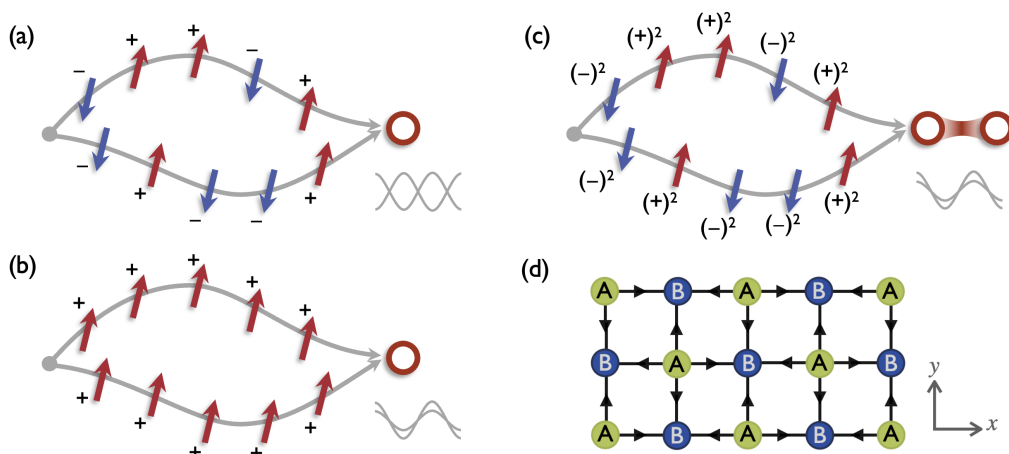


FIG. 3. (a)-(c) Schematic illustration of the \mathbb{Z}_2 Berry phase in the bosonic t - J model. The gray curves represent the worldlines of holes (hollow circles) passing through the spin background (red and blue arrows). (a) A single hole hopping on a generic spin background will accumulate a string of \mathbb{Z}_2 phases, with the sign determined by the orientation of the spin exchanged with the hole. The phases corresponding to different paths are different in general, leading to a disordered phase and destructive interference among different paths and hence the single-hole motion is strongly suppressed. (b) A single hole hopping on an FM background will accumulate an identical phase, so all paths contribute constructively and the coherence of single-hole motion can be restored. (c) Constructive interference can also be realized by the “in-tandem” motion of a hole pair on a generic spin background, as the \mathbb{Z}_2 phases created by the front hole can always be canceled with the identical phases created by the back hole. This restoration of coherence by the hole-pair motion leads to the emergence of the pairing order in the bosonic t - J model. (d) As the fluctuating Berry phases can be effectively canceled out by forming hole pairs, the phase of the pairing order is just determined by the residual static Marshall sign of the pair operator, resulting in the π -PDW. The black arrows on the links represent the sign pattern $(-1)^{i+\alpha}$ for the singlet pair operator $\Delta_{i\alpha}$ under the Marshall basis. Specifically, if α takes the same direction as the arrow, $\Delta_{i\alpha}$ has a positive sign under the Marshall basis. The yellow and blue circles represent the A and B sublattices, respectively.

which is known as the phase string [11–13]. N_{\downarrow}^h accounts for the total number of mutual exchanges between holes and \downarrow spins in a closed loop C . In other words, as illustrated in Fig. 3(a), the single hole hopping can accumulate a \mathbb{Z}_2 Berry phase with the sign determined by the orientation of the spin that is exchanged with the hole—positive for spin-up and negative for spin-down. In fact, this finding is broadly applicable to other strongly correlated systems, such as the fermionic t - J and Hubbard model [13, 64–67], where this emergent sign structure is an exclusive consequence of the Mottness independent of model details. In particular, for the bosonic t - J model, $(-1)^{N_{\downarrow}^h}$ is the *only* nontrivial sign structure, whereas, in the fermionic t - J model, the additional fermionic signs of dopants are also present.

Consequently, the coherence of a single hole is strongly disrupted by destructive interference of such a Berry phase that depends on the fluctuating spin configurations in the AFM background as illustrated in Fig. 3(a). This theoretical insight is corroborated by the DMRG results, which show a rapid decay in the single-particle Green’s function $G_{\sigma}(r)$ at small doping in Fig. 2(b). However, the phase frustration can be significantly canceled by the formation of tightly bound hole pairs in an “in-tandem” motion, where one hole always follows the other, as depicted in Fig. 3(c). Here the string of phases created by the front hole is compensated by the back hole, result-

ing in coherent hole pairs that can further condense to a BEC. Moreover, the pairing order parameter $\langle \Delta_{i\alpha} \rangle$ will further acquire a spatial modulation $(-1)^{i+\alpha}$ stemming from the static Marshall sign in the pair operator, as depicted in Fig. 3(d), giving rise to the π -PDW observed by DMRG, which is intertwined with the AFM order. Here $(-1)^i$ takes (∓ 1) for sublattice A and B respectively.

Alternatively, if the spin background is fully polarized to an FM order as shown in Fig. 3(b), one has $\tau_C = 1$ such that the phase coherence of the single-hole motion can be fully restored to realize a superfluid. In other words, a dominant hopping energy at larger doping forces the spins to go into an FM order, leading to the FM-SF phase found in Fig. 1(a). See Methods and Supplemental Information for the more detailed explanations [57].

Sign-problem-free: the bosonic σt - J model

To further showcase the critical phase frustration effect, one can artificially turn it off by modifying the hopping term H_t to

$$H_{\sigma t} = -t \sum_{(ij),\sigma} \sigma \left(B_{i\sigma}^{\dagger} B_{j\sigma} + \text{H.c.} \right). \quad (5)$$

The resulting bosonic σt - J model, $H_{\sigma t-J} = \mathcal{P}_s(H_{\sigma t} + H_J)\mathcal{P}_s$, can be shown [57] to have the same partition function in Eq. (3) except for $\tau_C \equiv 1$, i.e., with the sign problem completely removed. It is interesting to note

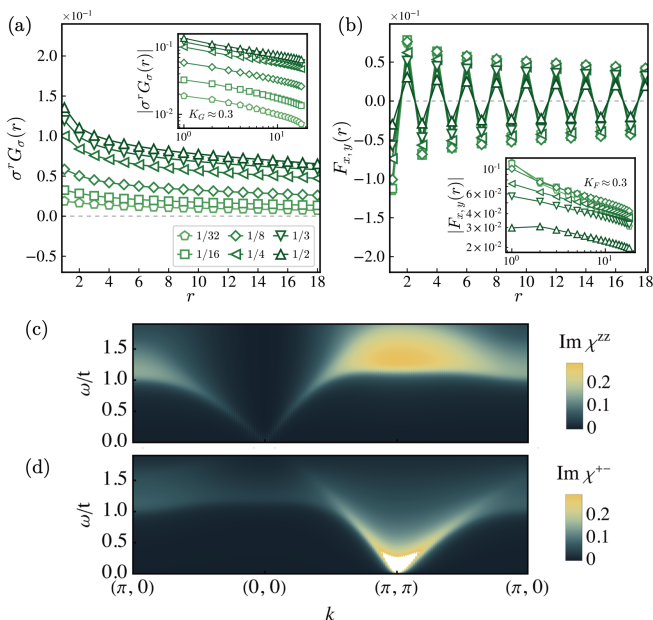


FIG. 4. (a) The single-particle Green’s function and (b) the spin-spin correlation along the $S^{x,y}$ direction in the ground state of the bosonic σt - J model obtained by DMRG simulations on cylinders of size 32×4 or 36×4 with $t/J = 3$ and varying doping level δ labeled by different markers. The spin dynamic susceptibility of the σt - J model at $t/J = 3$ and $\delta = 1/12$ by the parton mean-field calculation along (c) the S^z component (d) the $S^{x,y}$ component.

that such a sign-problem-free model is equivalent to the effective model of the spin-1/2 hard-core Bose-Hubbard model in the large- U limit (Methods).

Without the phase frustration, the dopants in the bosonic σt - J model can propagate coherently and hence undergo a BEC, as evidenced by the DMRG results in Fig. 4(a) [68–71], which is similar to the case of the FM-SF phase in the bosonic t - J model. In contrast to the latter, however, the AFM order here remains robust within the $S^{x,y}$ plane [cf. Fig. 4(b)]. Namely, the mutual entanglement between the spin background and the dopants vanishes with $\tau_C = 1$, leading to an effective decoupling between them. Note that the no-double-occupancy constraint due to the large U is still present, which does lead to the disorder in the S^z direction by the free motion of single dopants [57]. Such a constraint can be effectively addressed using a conventional parton mean-field scheme (Methods), based on which we show that at arbitrary non-zero doping, the bosons with opposite spins undergo BEC at zero temperature separately at the $(0, 0)$ and (π, π) momenta respectively. The spin spectrums at $\delta = 1/12$ are shown in Figs. 4(c) and (d), indicating an AFM order in the $S^{x,y}$ plane in good agreement with the DMRG calculations.

Discussion

In this work, we show that a quantum interference effect governs the physics in the bosonic t - J model. Specifi-

cally, the destructive interference caused by the \mathbb{Z}_2 Berry phase can significantly hinder the propagation of individual bosonic dopants in an AFM background. However, by forming tightly bound pairs, the doped holes can effectively eliminate such quantum frustration to restore phase coherence and then condense. This leads to an exotic pairing mechanism due to strong correlation effects beyond the no-double-occupancy constraint. It predicts a supersolid in which a PDW order coexists with the long-range AFM order at small doping. At larger doping, the same mechanism can enforce the spin background to transit to an FM order such that the single bosonic dopants become coherent to condense into a superfluid. These novel states are promising to be straightforwardly observed on ultracold Rydberg atom platforms [40, 42, 56, 57]. We point out that although related, the pairing mechanism discussed here differs from the mechanism purely based on the mismatch of NN spins caused by the hopping of doped holes. As an example, the ground state of the bosonic t - J_z model is found to be a superfluid [71] instead of a pairing order found here.

To a certain extent, the pairing mechanism here is analogous to the flat-band SC [72–74] in Moiré systems and other dispersionless systems, where the kinetic energy of single electrons is quenched due to interference effects while electron pairs can experience a different interference pattern to restore the superfluid density. However, unlike the flat-band SC where the pairing still needs to be mediated by bosonic fluctuations and can be understood through semi-classical relaxation scenarios, the pairing mechanism introduced in this work is rooted in quantum many-body interference itself. For Moiré systems, exotic-lattice systems, and the Hofstadter model, the interference patterns are static, dictated by lattice geometry or external field, allowing destructive interference to be effectively “neutralized” by expanding the unit cell, rendering it imperceptible at long wavelengths. By contrast, the quantum interference discussed here depends on the fluctuating background spins and hence is inherently *dynamic*, cannot be effectively removed, and remains significant even in the infrared limit.

The present bosonic model only differs from the well-known fermionic t - J model by the statistics of dopants. An additional fermionic sign structure will appear in the partition function of the latter. Two models are equivalent at half-filling and in the presence of one hole, but predict dramatically different phases at finite doping. In the latter, the fermionic statistics is expected to play an important role involving the overlap of hole pairs in a fashion of the BEC-BCS crossover with a partial recurrence of the phase frustration. The subsequent competing orders of charge stripe and short-range AFM [14] will replace the AFM-PDW state found in the present bosonic model, even though the hole pairing is still present. Given a similar pairing mechanism, the bosonic model can thus provide a different perspective and new insights into the nature of the complex phase diagram emerging in the fermionic doped Mott insulators that may be closely re-

lated to the high- T_c cuprate superconductors.

Methods

Density matrix renormalization group algorithm

We implement two DMRG schemes independently to obtain reliable results: (i) Grand canonical ensemble (GCE) where spontaneous $U(1)$ symmetry breaking is allowed giving rise to non-zero order parameters of pairing or single-particle condensation [26, 27]. A chemical potential μ is introduced to control the doping level δ indirectly. (ii) Canonical ensemble (CE) where the charge- $U(1)$ and spin- $U(1)$ symmetry are imposed to fix the total particle number and total spin S^z . The phases of matter are determined by computing long-distance correlation functions [17–25]. The bond dimensions are kept up to $D = 16000$ in the CE simulations to obtain accurate results with truncation error $\epsilon \lesssim 5 \times 10^{-6}$, while up to $D = 4000$ in the GCE simulations only to measure local properties on the natural ground states within broken symmetry plateaus [26, 27]. A variety of simulations is performed with different starting states and temporary pinning fields to avoid being stuck in metastable states. The spin- $U(1)$ symmetry is imposed in some of the GCE simulations in the AFM-PDW phase to speed up the computations and control the symmetry-breaking axis. Our primary focus is the GCE simulations for width-8 systems and the CE simulations for width-4 systems, which yield consistent phase diagrams. Other scenarios like width-2 and width-6 systems are also simulated in certain cases to support our conclusions further. We exploit either cylindrical boundary conditions (periodic in the \hat{y} direction and open in the \hat{x} direction) like the 32×8 cylinder in Fig. 1(b) or fully open boundary conditions (open in both the \hat{x} and \hat{y} directions) like the 8×8 square in Fig. 1(a) and the 32×6 lattice in Fig. 1(c). See Supplementary Section V [57] for further technical details, data analyses, and additional numerical results.

Parton mean-field approach

We introduce the following parton construction scheme for the bosonic σt - J model

$$B_i = b_{i\sigma} h_i^\dagger \quad (6)$$

where $b_{i\sigma}$ denotes the bosonic spinon of spin σ and h_i^\dagger denotes the bosonic holon. Then, the bosonic σt - J model in Eq. (5) can be expressed as follows:

$$H_{\sigma t-J} = t \sum_{\langle ij \rangle, \sigma} \sigma \hat{\chi}_{ij, \sigma} \hat{\kappa}_{ij}^\dagger + \text{H.c.} - \frac{J}{2} \sum_{ij} \hat{\Delta}_{ij}^\dagger \hat{\Delta}_{ij} \quad (7)$$

where

$$\begin{aligned} \hat{\kappa}_{ij} &= h_i^\dagger h_j \\ \hat{\chi}_{ij, \sigma} &= b_{i, \alpha}^\dagger b_{j, \sigma} \\ \hat{\Delta}_{ij} &= \sum_{\sigma} \sigma b_{i, \sigma} b_{j, -\sigma}, \end{aligned} \quad (8)$$

Based on the mean-field ansatz $\hat{\kappa}_{ij} = i\kappa$, $\hat{\chi}_{ij, \sigma} = i\sigma\chi$, and $\hat{\Delta}_{ij} = i\Delta$, the Hamiltonian (7) at the mean-field

level can be decomposed into the holon part H_h with the form of $H_h = \sum_k E_k^h h_k^\dagger h_k$, and the spinon part H_b , with the form of

$$H_b = \sum_{k, \sigma} \sigma \xi_k^b b_{k, \sigma}^\dagger b_{k, \sigma} + \sum_k \Delta_k (b_{-k, \downarrow} b_{k, \uparrow} + \text{H.c.}) \quad (9)$$

where $\xi_k^b = -2t\kappa\mathcal{E}_k + \lambda$ and $\Delta_k = J\Delta\mathcal{E}_k$, with $\mathcal{E}_k = \sin k_x + \sin k_y$. The dispersion for holon is given by $E_k^h = -4t\chi\mathcal{E}_k - \mu$. Similarly, from Eq. (9), by introducing the Bogoliubov transformation, we obtain the spinon dispersion: $E_k^b = \sqrt{\lambda_k^2 - \Delta_k^2}$ where $\lambda_k = \lambda - 2t\kappa\mathcal{E}_k$ and $\Delta_k = J\Delta\mathcal{E}_k$. The magnitude of χ , κ and Δ can be determined via the self-consistent calculation [57], indicating that both holon and spinons tend to be gapless, i.e., condensation, at the zero temperature. Note that, here the parton construction is just used to analyze the instability towards ordered states, i.e., confinement phase, at low temperatures, so that the gauge fluctuation effects in usual parton construction involving deconfined particles, do not need to be included here.

From H_b in Eq. (9), one can obtain the conventional and anomalous Green's functions for the spinons. By the relation $S_i^\gamma = b_{i, \sigma}^\dagger \tau_{\sigma\sigma'}^\gamma b_{i, \sigma'}/2$, the spin correlation in momentum and frequency space with the form

$$\chi^{\gamma\gamma'}(k, i\omega_n) = \int_0^\beta d\tau \sum_i e^{i(\omega_n\tau - k \cdot r)} \left\langle \hat{T} S_{i+r}^\gamma(\tau) S_i^{\gamma'}(0) \right\rangle, \quad (10)$$

can be expressed by the convolution of Green's function of spinons. See Supplementary Section IV [57] for the detailed derivation.

Quantum frustration analysis

The partition function of a generic quantum system $Z = \text{Tr} e^{-\beta H}$ can be expanded as a summation over closed paths of imaginary-time evolution [75]

$$Z = \sum_{n=0}^{\infty} \sum_{\{\alpha\}_n} \frac{\beta^n}{n!} \prod_{k=0}^{n-1} \langle \alpha_{k+1} | (-H) | \alpha_k \rangle, \quad (11)$$

where each $|\alpha_i\rangle$ runs over a complete basis of the Hilbert space, e.g., the real-space Fock basis. Each time series of states $\{\alpha\}_n$ should satisfy the temporal periodic boundary condition $|\alpha_n\rangle = |\alpha_0\rangle$. Each non-zero matrix element $\langle \alpha_{k+1} | (-H) | \alpha_k \rangle$ describes a single nontrivial evolution step. By decomposing matrix elements into magnitudes and phases (signs) and multiplying them respectively along each evolution path C , the partition function can be written as a path-integral-type summation

$$Z = \sum_C \tau_C W[C], \quad (12)$$

where τ_C and $W[C]$ represent the accumulated phase factor and the non-negative weight respectively. The expectation values of observables including various correlation functions can also be expanded as in Eq. (11) but

with extra operators inserted. There are other expansion schemes besides the direct series expansion used here, such as those in the auxiliary-field quantum Monte Carlo algorithm for interacting fermion systems, but they can still be written in the form of amplitude-phase summation like in Eq. (12). The phase factor τ_C captures the possible quantum interference among different evolution paths, or say the “quantumness” of the system under the expansion scheme. If τ_C is positive-definite, the quantum system is effectively mapped to a classical system and can be solved by Monte Carlo sampling methods. Otherwise, we say there is quantum frustration or a “sign (phase) problem”, especially when the phase strongly fluctuates. Quantum frustration is not only a crucial algorithmic problem in quantum many-body physics but also plays a critical role in determining the low-energy physics of corresponding models [76]. Interestingly, this frustration phase can be regarded as a generalized discrete version of the Berry phase action in the continuous path integral formalism of conventional models [6, 77]. It is an “adiabatic” phase accumulated during an evolution loop that cannot be gauged away and is independent of the evolution speed, in contrast to the dynamical phase stemming from the exponentiated imaginary unit i in the real-time evolution.

For the undoped AFM Heisenberg model H_J on bipartite lattices, the phase factor τ_C is positive-definite because despite that the non-zero off-diagonal matrix element $\langle \alpha_{k+1} | (-S_i^+ S_j^-) | \alpha_k \rangle$ is always negative, an even number of spin exchanges is required in every allowed evolution path to satisfy the temporal periodicity. This can be seen more explicitly and locally by transforming the Hamiltonian into a stochastic form according to the so-called Marshall sign rule [6]. Namely, we perform the following gauge transformation

$$U_{\text{Ms}} = (-1)^{N_{\text{A}}^{\downarrow}} = \prod_{i \in \text{A}} e^{i\pi n_{i\downarrow}}, \quad (13)$$

which counts the parity of the total number of \downarrow spins $N_{\text{A}}^{\downarrow}$ on sublattice A (here the choices of sublattice and \downarrow or \uparrow spins are arbitrary). The transformed Heisenberg interaction carries an extra minus sign for the spin-flip process

$$\begin{aligned} H_J^- &= U_{\text{Ms}} H_J U_{\text{Ms}}^\dagger \\ &= J \sum_{\langle ij \rangle} \left(-S_i^x S_j^x - S_i^y S_j^y + S_i^z S_j^z - \frac{1}{4} n_i n_j \right), \end{aligned} \quad (14)$$

so that all non-zero matrix elements in Eq. (11) become positive (“stochastic”), resulting in a positive-definite τ_C . Note that each contribution in Eq. (12) is invariant under a phase transformation like U_{Ms} .

For the doped AFM bosonic t - J model, quantum frustration emerges upon doping holes because the number of spin exchanges is not necessarily even anymore due to the

additional hole-spin exchange process. If one removes the negative sign in the spin exchange process by U_{Ms} , another negative sign will arise in the transformed hopping term $H_{\sigma t} = U_{\text{Ms}} H_t U_{\text{Ms}}^\dagger$ correspondingly, where the phase factor takes the form of Eq. (4) as the exchange of a hole and a \downarrow spin contributes a negative sign. If one focuses on the “worldline” of a single hole, a string of \mathbb{Z}_2 phases $(\pm 1) \times (\pm 1) \times \dots \times (\pm 1)$ will be picked up by the moving hole from the spin background depending on the orientation of the spin exchanged with the hole [11, 13]. We emphasize that the key advantage of the Marshall transformation is that it allows us to focus on the motion of holes by rendering the spin-flip process positive-definite, thereby eliminating the need to account for the phases arising from the realignment of the spin background. In other words, the frustration phase in the form of Eq. (4) treats doped holes as fundamental objects. See Supplementary Section II [57] for the detailed derivation and discussion.

Bosonic σt - J and Bose-Hubbard model

If an additional negative sign is artificially attached to the exchange process of holes and \downarrow spins to cancel the spin-dependent hopping sign transferred from the spin-exchange process by U_{Ms} , the resulting Hamiltonian will contain no quantum frustration anymore, leading to the bosonic σt - J model discussed in the main text. Alternatively, the bosonic σt - J model can be obtained less artificially from the effective model of the spin-1/2 hard-core Bose-Hubbard model. The Hamiltonian of this Bose-Hubbard model reads $H_{t-U} = H_t + H_U$ where H_t is the same hopping term as in Eq. (1) and

$$H_U = U \sum_i n_{i\uparrow} n_{i\downarrow}, \quad (15)$$

is the on-site Hubbard repulsion. In contrast to the fermionic case, the effective Hamiltonian of this Bose-Hubbard model in the large- U limit will lead to a ferromagnetic spin-exchange interaction [78] in the exact form of H_J^- as in Eq. (14). Namely, the effective Hamiltonian reads $H_{t-J}^- = \mathcal{P}_s (H_t + H_J^-) \mathcal{P}_s$. After performing the Marshall transformation U_{Ms} , the resulting Hamiltonian is exactly the bosonic σt - J model $H_{\sigma t-J} = U_{\text{Ms}} H_{t-J}^- U_{\text{Ms}}^\dagger$. Thus, the correlation functions on the ground states of the two models are closely related to each other by applying U_{Ms} to the observables. Especially, the pure “charge” properties are exactly the same, such as the hole-hole density correlation $D_h(r)$ in Fig. 1(c). The sign-problem-free property of the bosonic σt - J model is hence a natural result from the sign-problem-free Bose-Hubbard model.

Data availability

The data generated and analyzed in this paper are available upon request to the authors.

Code availability

The numerical codes in this paper are available upon request to the authors.

-
- [1] B. Keimer, S. A. Kivelson, M. R. Norman, S. Uchida, and J. Zaanen, From quantum matter to high-temperature superconductivity in copper oxides, *Nature* **518**, 179 (2015).
- [2] P. W. Anderson, The Resonating Valence Bond State in La_2CuO_4 and Superconductivity, *Science* **235**, 1196 (1987).
- [3] P. A. Lee, N. Nagaosa, and X.-G. Wen, Doping a Mott insulator: Physics of high-temperature superconductivity, *Reviews of Modern Physics* **78**, 17 (2006).
- [4] J. Hubbard, Electron correlations in narrow energy bands, *Proc. R. Soc. Lond. A* **276**, 238 (1963).
- [5] F. C. Zhang and T. M. Rice, Effective Hamiltonian for the superconducting Cu oxides, *Physical Review B* **37**, 3759 (1988).
- [6] A. Auerbach, *Interacting electrons and quantum magnetism* (Springer New York, 2012).
- [7] M. Ogata and H. Fukuyama, The t - J model for the oxide high- T_c superconductors, *Reports on Progress in Physics* **71**, 036501 (2008).
- [8] D. P. Arovas, E. Berg, S. A. Kivelson, and S. Raghu, The Hubbard Model, *Annual Review of Condensed Matter Physics* **13**, 239 (2022).
- [9] P. W. Anderson, G. Baskaran, Z. Zou, and T. Hsu, Resonating-valence-bond theory of phase transitions and superconductivity in La_2CuO_4 -based compounds, *Physical Review Letters* **58**, 2790 (1987).
- [10] S. Liang, B. Doucot, and P. W. Anderson, Some New variational resonating-valence-bond-type wave functions for the spin-1/2 antiferromagnetic heisenberg model on a square lattice, *Physical Review Letters* **61**, 365 (1988).
- [11] D. N. Sheng, Y. C. Chen, and Z. Y. Weng, Phase string effect in a doped antiferromagnet, *Physical Review Letters* **77**, 5102 (1996).
- [12] Z. Y. Weng, D. N. Sheng, Y.-C. Chen, and C. S. Ting, Phase string effect in the t - J model: General theory, *Physical Review B* **55**, 3894 (1997).
- [13] K. Wu, Z. Y. Weng, and J. Zaanen, Sign structure of the t - J model, *Physical Review B* **77**, 155102 (2008).
- [14] E. Fradkin, S. A. Kivelson, and J. M. Tranquada, Colloquium: Theory of intertwined orders in high temperature superconductors, *Rev. Mod. Phys.* **87**, 457 (2015).
- [15] B.-X. Zheng, C.-M. Chung, P. Corboz, G. Ehlers, M.-P. Qin, R. M. Noack, H. Shi, S. R. White, S. Zhang, and G. K.-L. Chan, Stripe order in the underdoped region of the two-dimensional Hubbard model, *Science* **358**, 1155 (2017).
- [16] E. W. Huang, C. B. Mendl, S. Liu, S. Johnston, H.-C. Jiang, B. Moritz, and T. P. Devereaux, Numerical evidence of fluctuating stripes in the normal state of high- T_c cuprate superconductors, *Science* **358**, 1161 (2017).
- [17] H.-C. Jiang, Z.-Y. Weng, and S. A. Kivelson, Superconductivity in the doped t - J model: Results for four-leg cylinders, *Physical Review B* **98**, 140505 (2018).
- [18] H.-C. Jiang and T. P. Devereaux, Superconductivity in the doped Hubbard model and its interplay with next-nearest hopping t' , *Science* **365**, 1424 (2019).
- [19] C.-M. Chung, M. Qin, S. Zhang, U. Schollwöck, and S. R. White, Plaquette versus ordinary d -wave pairing in the t' -Hubbard model on a width-4 cylinder, *Physical Review B* **102**, 041106 (2020).
- [20] Y.-F. Jiang, J. Zaanen, T. P. Devereaux, and H.-C. Jiang, Ground state phase diagram of the doped Hubbard model on the four-leg cylinder, *Physical Review Research* **2**, 033073 (2020).
- [21] M. Qin, C.-M. Chung, H. Shi, E. Vitali, C. Hubig, U. Schollwöck, S. R. White, and S. Zhang, Absence of Superconductivity in the Pure Two-Dimensional Hubbard Model, *Physical Review X* **10**, 031016 (2020).
- [22] S. Gong, W. Zhu, and D. N. Sheng, Robust d -Wave Superconductivity in the Square-Lattice t - J Model, *Physical Review Letters* **127**, 097003 (2021).
- [23] X. Lu, D.-W. Qu, Y. Qi, W. Li, and S.-S. Gong, Ground-state phase diagram of the extended two-leg t - J ladder, *Physical Review B* **107**, 125114 (2023).
- [24] X. Lu, F. Chen, W. Zhu, D. N. Sheng, and S.-S. Gong, Emergent Superconductivity and Competing Charge Orders in Hole-Doped Square-Lattice t - J Model, *Physical Review Letters* **1**, 066002 (2024).
- [25] Y.-F. Jiang, T. P. Devereaux, and H.-C. Jiang, Ground-state phase diagram and superconductivity of the doped Hubbard model on six-leg square cylinders, *Physical Review B* **109**, 085121 (2024).
- [26] S. Jiang, D. J. Scalapino, and S. R. White, Ground State Phase Diagram of the t - t' - J model, *Proceedings of the National Academy of Sciences* **118**, 1 (2021).
- [27] F. Chen, F. D. M. Haldane, and D. N. Sheng, D -Wave and Pair-Density-Wave Superconductivity in the Square-Lattice t - J Model, *arXiv:2311.15092* (2023).
- [28] D.-W. Qu, B.-B. Chen, X. Lu, Q. Li, Y. Qi, S.-S. Gong, W. Li, and G. Su, High- T_c Superconductivity and Finite-Temperature Phase Diagram of the t - t' - J Model, *arXiv:2211.06322* (2022).
- [29] H. Xu, C.-M. Chung, M. Qin, U. Schollwöck, S. R. White, and S. Zhang, Coexistence of superconductivity with partially filled stripes in the Hubbard model, *Science* **384**, eadh7691 (2024).
- [30] A. Wietek, Y.-Y. He, S. R. White, A. Georges, and E. M. Stoudenmire, Stripes, Antiferromagnetism, and the Pseudogap in the Doped Hubbard Model at Finite Temperature, *Physical Review X* **11**, 031007 (2021).
- [31] Q. Li, Y. Gao, Y.-Y. He, Y. Qi, B.-B. Chen, and W. Li, Tangent Space Approach for Thermal Tensor Network Simulations of the 2D Hubbard Model, *Physical Review Letters* **130**, 226502 (2023).
- [32] A. Bohrdt, L. Homeier, C. Reinmoser, E. Demler, and F. Grusdt, Exploration of doped quantum magnets with ultracold atoms, *Annals of Physics* **435**, 168651 (2021).
- [33] L. W. Cheuk, M. A. Nichols, K. R. Lawrence, M. Okan, H. Zhang, E. Khatami, N. Trivedi, T. Paiva, M. Rigol, and M. W. Zwierlein, Observation of spatial charge and spin correlations in the 2D Fermi-Hubbard model, *Science* **353**, 1260 (2016).
- [34] P. T. Brown, D. Mitra, E. Guardado-Sanchez, P. Schauß, S. S. Kondov, E. Khatami, T. Paiva, N. Trivedi, D. A. Huse, and W. S. Bakr, Spin-imbalance in a 2D Fermi-Hubbard system, *Science* **357**, 1385 (2017).
- [35] A. Mazurenko, C. S. Chiu, G. Ji, M. F. Parsons, M. Kanász-Nagy, R. Schmidt, F. Grusdt, E. Demler, D. Greif, and M. Greiner, A cold-atom Fermi-Hubbard antiferromagnet, *Nature* **545**, 462 (2017).
- [36] P. T. Brown, D. Mitra, E. Guardado-Sanchez,

- R. Nourafkan, A. Reymbaut, C.-D. Hébert, S. Bergeron, A.-M. S. Tremblay, J. Kokalj, D. A. Huse, P. Schauß, and W. S. Bakr, Bad metallic transport in a cold atom Fermi-Hubbard system, *Science* **363**, 379 (2019).
- [37] J. Koepsell, J. Vijayan, P. Sompet, F. Grusdt, T. A. Hilker, E. Demler, G. Salomon, I. Bloch, and C. Gross, Imaging magnetic polarons in the doped Fermi-Hubbard model, *Nature* **572**, 358 (2019).
- [38] M. A. Nichols, L. W. Cheuk, M. Okan, T. R. Hartke, E. Mendez, T. Senthil, E. Khatami, H. Zhang, and M. W. Zwierlein, Spin transport in a Mott insulator of ultracold fermions, *Science* **363**, 383 (2019).
- [39] M. Gall, C. F. Chan, N. Wurz, and M. Köhl, Simulating a Mott Insulator Using Attractive Interaction, *Physical Review Letters* **124**, 010403 (2020).
- [40] J. Koepsell, D. Bourgund, P. Sompet, S. Hirthe, A. Bohrdt, Y. Wang, F. Grusdt, E. Demler, G. Salomon, C. Gross, and I. Bloch, Microscopic evolution of doped Mott insulators from polaronic metal to Fermi liquid, *Science* **374**, 82 (2021).
- [41] M. Xu, L. H. Kendrick, A. Kale, Y. Gang, G. Ji, R. T. Scalettar, M. Lebrat, and M. Greiner, Frustration- and doping-induced magnetism in a Fermi-Hubbard simulator, *Nature* **620**, 971 (2023).
- [42] M. Lebrat, M. Xu, L. H. Kendrick, A. Kale, Y. Gang, P. Seetharaman, I. Morera, E. Khatami, E. Demler, and M. Greiner, Observation of Nagaoka polarons in a Fermi-Hubbard quantum simulator, *Nature* **629**, 317 (2024).
- [43] J. Vijayan, P. Sompet, G. Salomon, J. Koepsell, S. Hirthe, A. Bohrdt, F. Grusdt, I. Bloch, and C. Gross, Time-resolved observation of spin-charge deconfinement in fermionic Hubbard chains, *Science* **367**, 186 (2020).
- [44] H. Sun, B. Yang, H.-Y. Wang, Z.-Y. Zhou, G.-X. Su, H.-N. Dai, Z.-S. Yuan, and J.-W. Pan, Realization of a bosonic antiferromagnet, *Nature Physics* **17**, 990 (2021).
- [45] P. Sompet, S. Hirthe, D. Bourgund, T. Chalopin, J. Bibo, J. Koepsell, P. Bojović, R. Verresen, F. Pollmann, G. Salomon, C. Gross, T. A. Hilker, and I. Bloch, Realizing the symmetry-protected Haldane phase in Fermi-Hubbard ladders, *Nature* **606**, 484 (2022).
- [46] T. Hartke, B. Oreg, C. Turnbaugh, N. Jia, and M. Zwierlein, Direct observation of nonlocal fermion pairing in an attractive Fermi-Hubbard gas, *Science* **381**, 82 (2023).
- [47] A. Browaeys and T. Lahaye, Many-body physics with individually controlled Rydberg atoms, *Nature Physics* **16**, 132 (2020).
- [48] D. Mitra, P. T. Brown, E. Guardado-Sanchez, S. S. Kondov, T. Devakul, D. A. Huse, P. Schauß, and W. S. Bakr, Quantum gas microscopy of an attractive Fermi-Hubbard system, *Nature Physics* **14**, 173 (2018).
- [49] F. Yang, S. Yang, and L. You, Quantum Transport of Rydberg Excitons with Synthetic Spin-Exchange Interactions, *Physical Review Letters* **123**, 063001 (2019).
- [50] P. N. Jepsen, J. Amato-Grill, I. Dimitrova, W. W. Ho, E. Demler, and W. Ketterle, Spin transport in a tunable Heisenberg model realized with ultracold atoms, *Nature* **588**, 403 (2020).
- [51] S. Ebadi, T. T. Wang, H. Levine, A. Keesling, G. Semeghini, A. Omran, D. Bluvstein, R. Samajdar, H. Pichler, W. W. Ho, S. Choi, S. Sachdev, M. Greiner, V. Vuletić, and M. D. Lukin, Quantum phases of matter on a 256-atom programmable quantum simulator, *Nature* **595**, 227 (2021).
- [52] G. Semeghini, H. Levine, A. Keesling, S. Ebadi, T. T. Wang, D. Bluvstein, R. Verresen, H. Pichler, M. Kalinowski, R. Samajdar, A. Omran, S. Sachdev, A. Vishwanath, M. Greiner, V. Vuletić, and M. D. Lukin, Probing topological spin liquids on a programmable quantum simulator, *Science* **374**, 1242 (2021).
- [53] C. Chen, G. Bornet, M. Bintz, G. Emperauger, L. Leclerc, V. S. Liu, P. Scholl, D. Barredo, J. Hauschild, S. Chatterjee, M. Schuler, A. M. Läuchli, M. P. Zaletel, T. Lahaye, N. Y. Yao, and A. Browaeys, Continuous symmetry breaking in a two-dimensional Rydberg array, *Nature* **616**, 691 (2023).
- [54] D. Bluvstein, H. Levine, G. Semeghini, T. T. Wang, S. Ebadi, M. Kalinowski, A. Keesling, N. Maskara, H. Pichler, M. Greiner, V. Vuletić, and M. D. Lukin, A quantum processor based on coherent transport of entangled atom arrays, *Nature* **604**, 451 (2022).
- [55] D. Bluvstein, S. J. Evered, A. A. Geim, S. H. Li, H. Zhou, T. Manovitz, S. Ebadi, M. Cain, M. Kalinowski, D. Hangleiter, J. P. Bonilla Ataides, N. Maskara, I. Cong, X. Gao, P. Sales Rodriguez, T. Karolyshyn, G. Semeghini, M. J. Gullans, M. Greiner, V. Vuletić, and M. D. Lukin, Logical quantum processor based on reconfigurable atom arrays, *Nature* **626**, 58 (2024).
- [56] L. Homeier, T. J. Harris, T. Blatz, S. Geier, S. Hollerith, U. Schollwöck, F. Grusdt, and A. Bohrdt, Antiferromagnetic Bosonic t - J Models and Their Quantum Simulation in Tweezer Arrays, *Physical Review Letters* **132**, 230401 (2024).
- [57] See Supplemental Material for detailed analytic derivation, further elaboration, and additional numerical results.
- [58] D. F. Agterberg, J. S. Davis, S. D. Edkins, E. Fradkin, D. J. Van Harlingen, S. A. Kivelson, P. A. Lee, L. Radzihovsky, J. M. Tranquada, and Y. Wang, The Physics of Pair-Density Waves: Cuprate Superconductors and Beyond, *Annual Review of Condensed Matter Physics* **11**, 231 (2020).
- [59] H.-C. Jiang, Pair density wave in the doped three-band Hubbard model on two-leg square cylinders, *Physical Review B* **107**, 214504 (2023).
- [60] H.-K. Zhang, R.-Y. Sun, and Z.-Y. Weng, Pair density wave characterized by a hidden string order parameter, *Physical Review B* **108**, 115136 (2023).
- [61] Z.-Y. Yue, Z.-T. Xu, S. Yang, and Z.-C. Gu, Pseudogap phase as fluctuating pair density wave, [arXiv:2404.16770](https://arxiv.org/abs/2404.16770) (2024).
- [62] M. P. A. Fisher, P. B. Weichman, G. Grinstein, and D. S. Fisher, Boson localization and the superfluid-insulator transition, *Phys. Rev. B* **40**, 546 (1989).
- [63] K. Sheshadri, H. R. Krishnamurthy, R. Pandit, and T. V. Ramakrishnan, Superfluid and insulating phases in an interacting-boson model: Mean-field theory and the rpa, *Europhysics Letters* **22**, 257 (1993).
- [64] X. Lu, J.-X. Zhang, S.-S. Gong, D. N. Sheng, and Z.-Y. Weng, Sign structure in the square-lattice t - J model and numerical consequences, [arXiv:2303.13498](https://arxiv.org/abs/2303.13498) (2023).
- [65] J.-X. Zhang, H.-K. Zhang, Y.-Z. You, and Z.-Y. Weng, Strong Pairing Originated from an Emergent \mathbb{Z}_2 Berry Phase in $\text{La}_3\text{Ni}_2\text{O}_7$, *Physical Review Letters* **133**, 126501 (2024).
- [66] L. Zhang and Z.-Y. Weng, Sign structure, electron fractionalization, and emergent gauge description of the Hubbard model, *Physical Review B* **90**, 165120 (2014).

- [67] J.-S. Xu, Z. Zhu, K. Wu, and Z.-Y. Weng, Hubbard model on a triangular lattice: The role of charge fluctuations, *Physical Review B* **109**, L081116 (2024).
- [68] M. Boninsegni, Phase Separation in Mixtures of Hard Core Bosons, *Physical Review Letters* **87**, 087201 (2001).
- [69] M. Boninsegni, Phase separation and stripes in a boson version of a doped quantum antiferromagnet, *Physical Review B* **65**, 134403 (2002).
- [70] M. Boninsegni and N. V. Prokof'ev, Phase diagram of an anisotropic bosonic t - J model, *Physical Review B* **77**, 092502 (2008).
- [71] J. Šmakov, C. D. Batista, and G. Ortiz, Stripes, Topological Order, and Deconfinement in a Planar t - J_z Model, *Physical Review Letters* **93**, 067201 (2004).
- [72] P. Törmä, S. Peotta, and B. A. Bernevig, Superconductivity, superfluidity and quantum geometry in twisted multilayer systems, *Nature Reviews Physics* **4**, 528 (2022).
- [73] S. Peotta and P. Törmä, Superfluidity in topologically nontrivial flat bands, *Nature Communications* **6** (2015).
- [74] S. A. Chen and K. T. Law, Ginzburg-landau theory of flat-band superconductors with quantum metric, *Phys. Rev. Lett.* **132**, 026002 (2024).
- [75] A. W. Sandvik, A. Avella, and F. Mancini, Computational Studies of Quantum Spin Systems, in *AIP Conference Proceedings*, Vol. 1297 (2010) pp. 135–338.
- [76] Y. Zhou, K. Kanoda, and T.-K. Ng, Quantum spin liquid states, *Reviews of Modern Physics* **89**, 025003 (2017).
- [77] A. Altland and B. D. Simons, Topology, in *Condensed Matter Field Theory* (Cambridge University Press, 2010) p. 496–601.
- [78] L.-M. Duan, E. Demler, and M. D. Lukin, Controlling Spin Exchange Interactions of Ultracold Atoms in Optical Lattices, *Physical Review Letters* **91**, 090402 (2003).

Acknowledgments

We acknowledge the stimulating discussions with Zhi-Jian Song and Yu-Peng Wang. H.-K.Z, J.-S.X., and Z.-Y.W. are supported by MOST of China (Grant No. 2021YFA1402101) and NSF of China (Grant No. 12347107); J.-X.Z was funded by the European Research Council (ERC) under the European Union's Horizon 2020 research and innovation program (Grant Agreement No. 853116, acronym TRANSPORT). This research was supported in part by grant NSF PHY-2309135 to the Kavli Institute for Theoretical Physics (KITP).

Author contributions

H.-K.Z., J.-X.Z., and Z.-Y.W. conceived the project, conducted theoretical analysis, and wrote the manuscript. H.-K.Z performed the numerical simulation. J.-X.Z. conducted the parton mean-field calculation. J.-S.X participated in the discussion.

Competing interests

The authors declare no competing interests.

Additional information

Supplementary information The online version contains supplementary material.

**Supplemental Material for
“Quantum-interference-induced pairing in antiferromagnetic bosonic t - J model”**

Contents

References	8
I. The effective model of the spinful hard-core Bose-Hubbard model	11
II. Quantum frustration analysis	14
A. Bosonic t - J model	14
B. Bosonic σt - J model	15
C. Spinful hard-core Bose-Hubbard model	16
D. Relation with the continuous Berry phase	16
III. Analysis on the phase of pairing order parameter	16
A. Pairing in bosonic systems	16
B. Pairing phase from the Marshall sign and constructive interference	17
IV. Parton construction of the bosonic σt - J model	18
A. Mean-field scheme	18
B. Spin response	20
V. Numerical details and additional simulation results	21
A. Numerical details	21
B. Additional simulation results	22
1. Correlation function analysis for the bosonic t - J model	22
2. Probing the phase of pairing	24
3. Density distributions	26
4. Correlation function analysis for the bosonic σt - J model	26
5. Hole-hole correlation in two-hole-doped systems	27
C. Measuring pair-pair correlations in cold atom simulations	27

I. The effective model of the spinful hard-core Bose-Hubbard model

In this section, we will derive the effective model of the spinful Bose-Hubbard model in the limit of $U \gg t$ and show that it is equivalent to the bosonic σt - J model investigated in this work under an on-site unitary (phase) transformation on bipartite lattices, similar to the derivation from the Fermi-Hubbard model to the standard fermionic t - J model via the second-order perturbation in the large U limit. The Hamiltonian of the one-band spinful hard-core Bose-Hubbard model reads

$$H_{t-U} = H_t + H_U = -t \sum_{\langle ij \rangle \sigma} \left(B_{i\sigma}^\dagger B_{j\sigma} + \text{h.c.} \right) + U \sum_i n_{i\uparrow} n_{i\downarrow}, \quad (\text{S1})$$

where $B_{i\sigma}^\dagger$ and $B_{i\sigma}$ are the creation and annihilation operators of a hard-core boson of spin $\sigma \in \{\uparrow, \downarrow\}$ at site i , respectively. The corresponding commutation relation is

$$\begin{aligned} [B_{i\sigma}, B_{j\sigma'}^\dagger] &= 0, \quad [B_{i\sigma}, B_{j\sigma'}] = 0, \quad \text{if } i \neq j \text{ or } \sigma \neq \sigma', \\ \{B_{i\sigma}, B_{j\sigma'}^\dagger\} &= 1, \quad \text{if } i = j \text{ and } \sigma = \sigma', \end{aligned} \quad (\text{S2})$$

or equivalently,

$$[B_{i\sigma}, B_{j\sigma'}^\dagger] = \delta_{ij} \delta_{\sigma\sigma'} \left(1 - 2B_{j\sigma'}^\dagger B_{i\sigma} \right), \quad [B_{i\sigma}, B_{j\sigma'}] = 0, \quad (\text{S3})$$

where δ_{ij} denotes the Kronecker delta function and the identity operator is omitted for simplicity and denoted as 1. $n_{i\sigma} = B_{i\sigma}^\dagger B_{i\sigma}$ is the particle density operator of spin σ at site i . We use $n_i = \sum_\sigma n_{i\sigma}$ to denote the total particle

density at site i . $t \geq 0$ is the hopping integral between the nearest-neighbor (NN) sites $\langle ij \rangle$ and $U \geq 0$ is the on-site Hubbard repulsion.

Suppose that the total particle number is below half-filling. In the limit of $U/t \rightarrow +\infty$, the ground states are highly degenerate, forming a subspace spanned by all possible no-double-occupied configurations. Denote the projector to this subspace as \mathcal{P}_s . According to the Brillouin-Wigner perturbation theory, the contributions to the effective Hamiltonian up to the second order are

$$\begin{aligned} H_{\text{eff}}^{(0)} &= \mathcal{P}_s H_U \mathcal{P}_s = 0, \\ H_{\text{eff}}^{(1)} &= \mathcal{P}_s H_t \mathcal{P}_s, \\ H_{\text{eff}}^{(2)} &= \mathcal{P}_s H_t \frac{1 - \mathcal{P}_s}{0 - H_U} H_t \mathcal{P}_s = -\frac{1}{U} \mathcal{P}_s H_t (1 - \mathcal{P}_s) H_t \mathcal{P}_s \\ &= -\frac{t^2}{U} \sum_{\langle ij \rangle \langle kl \rangle \sigma \sigma'} \mathcal{P}_s \left(B_{i\sigma}^\dagger B_{j\sigma} + \text{h.c.} \right) (1 - \mathcal{P}_s) \left(B_{k\sigma'}^\dagger B_{l\sigma'} + \text{h.c.} \right) \mathcal{P}_s. \end{aligned} \quad (\text{S4})$$

In the second-order contribution, the successive action of the projectors \mathcal{P}_s , $(1 - \mathcal{P}_s)$, and \mathcal{P}_s results in the surviving terms in H_t must map a no-double-occupied configuration to a double-occupied configuration and then back to a no-double-occupied configuration. Hence, H_U^{-1} directly becomes $1/U$ and the two links $\langle ij \rangle$ and $\langle kl \rangle$ must have overlaps. In the following, we only consider the cases where the two links completely coincide $\langle ij \rangle = \langle kl \rangle$, i.e., the cases where the two links overlap by only one site are omitted, as in the derivation of the standard fermionic t - J model. Hence, for each link $\langle ij \rangle$, the effect of the projector $(1 - \mathcal{P}_s)$ can be equivalently represented by a factor $n_i n_j$ just after the first (rightmost) \mathcal{P}_s , which means that only the configuration with singly-occupied sites i, j can survive and then naturally leads to a double-occupied configuration after the action of H_t . Thus, the second-order contribution becomes

$$H_{\text{eff}}^{(2)'} = -\frac{t^2}{U} \sum_{\langle ij \rangle \sigma \sigma'} \mathcal{P}_s \left(B_{i\sigma}^\dagger B_{j\sigma} + \text{h.c.} \right) \left(B_{i\sigma'}^\dagger B_{j\sigma'} + \text{h.c.} \right) n_i n_j \mathcal{P}_s. \quad (\text{S5})$$

The terms in the summation on a single link $\langle ij \rangle$ can be expressed as

$$\begin{aligned} & \mathcal{P}_s \left(\sum_{\sigma} B_{i\sigma}^\dagger B_{j\sigma} + \text{h.c.} \right)^2 n_i n_j \mathcal{P}_s \\ &= \sum_{\sigma \sigma'} \mathcal{P}_s \left(B_{i\sigma}^\dagger B_{j\sigma} B_{i\sigma'}^\dagger B_{j\sigma'} + B_{i\sigma}^\dagger B_{j\sigma} B_{j\sigma'}^\dagger B_{i\sigma'} + B_{j\sigma}^\dagger B_{i\sigma} B_{i\sigma'}^\dagger B_{j\sigma'} + B_{j\sigma}^\dagger B_{i\sigma} B_{j\sigma'}^\dagger B_{i\sigma'} \right) n_i n_j \mathcal{P}_s \\ &= \sum_{\sigma \sigma'} \mathcal{P}_s \left(B_{i\sigma}^\dagger B_{i\sigma'} (\delta_{\sigma\sigma'} - (2\delta_{\sigma\sigma'} - 1) B_{j\sigma'}^\dagger B_{j\sigma}) + (\delta_{\sigma\sigma'} - (2\delta_{\sigma\sigma'} - 1) B_{i\sigma'}^\dagger B_{i\sigma}) B_{j\sigma}^\dagger B_{j\sigma'} \right) n_i n_j \mathcal{P}_s, \\ &= \mathcal{P}_s \left(n_i + n_j + 2 \sum_{\sigma \sigma'} B_{i\sigma}^\dagger B_{i\sigma'} B_{j\sigma'}^\dagger B_{j\sigma} - 4 \sum_{\sigma} n_{i\sigma} n_{j\sigma} \right) n_i n_j \mathcal{P}_s. \end{aligned} \quad (\text{S6})$$

Note that the first and last terms in the second line vanish due to the projector \mathcal{P}_s . Compared to the fermionic case, the sign of the exchange term $2 \sum_{\sigma \sigma'} B_{i\sigma}^\dagger B_{i\sigma'} B_{j\sigma'}^\dagger B_{j\sigma}$ is reversed and there is an additional term $-4 \sum_{\sigma} n_{i\sigma} n_{j\sigma}$. The exchange term can be rewritten via the Schwinger boson representation of the spin operator

$$\mathbf{S}_i = (S_i^x, S_i^y, S_i^z) = \frac{1}{2} \sum_{\sigma \sigma'} B_{i\sigma}^\dagger \boldsymbol{\tau}_{\sigma\sigma'} B_{i\sigma'}, \quad (\text{S7})$$

as

$$2 \sum_{\sigma \sigma'} B_{i\sigma}^\dagger B_{i\sigma'} B_{j\sigma'}^\dagger B_{j\sigma} = 4 \mathbf{S}_i \cdot \mathbf{S}_j + n_i n_j. \quad (\text{S8})$$

by use of the Pauli decomposition of the swap operation

$$2\delta_{\sigma\rho'}\delta_{\sigma'\rho} = \boldsymbol{\tau}_{\sigma\sigma'} \cdot \boldsymbol{\tau}_{\rho\rho'} + \delta_{\sigma\sigma'}\delta_{\rho\rho'}, \quad (\text{S9})$$

where $\boldsymbol{\tau}_{\sigma\sigma'}$ denote the vector composed of the three Pauli matrices. Hence, the second-order contribution to the effective Hamiltonian is

$$H_{\text{eff}}^{(2)'} = -J \mathcal{P}_s \left(\mathbf{S}_i \cdot \mathbf{S}_j + \frac{3}{4} n_i n_j - \sum_{\sigma} n_{i\sigma} n_{j\sigma} \right) \mathcal{P}_s, \quad (\text{S10})$$

where the spin-exchange coupling constant is still $J = 4t^2/U$. However, the coupling term $\mathbf{S}_i \cdot \mathbf{S}_j$ becomes ferromagnetic, which is completely different from the fermionic case. Recombining the terms in Eq. (S10) using the identity

$$4S_i^z S_j^z + n_i n_j = \sum_{\sigma\sigma'} (\sigma\sigma' + 1) n_{i\sigma} n_{j\sigma'} = \sum_{\sigma\sigma'} 2\delta_{\sigma\sigma'} n_{i\sigma} n_{j\sigma'} = 2 \sum_{\sigma} n_{i\sigma} n_{j\sigma}, \quad (\text{S11})$$

will obtain

$$\begin{aligned} \mathbf{S}_i \cdot \mathbf{S}_j + \frac{3}{4} n_i n_j - \sum_{\sigma} n_{i\sigma} n_{j\sigma} &= \mathbf{S}_i \cdot \mathbf{S}_j + \frac{3}{4} n_i n_j - \frac{1}{2} (4S_i^z S_j^z + n_i n_j) \\ &= S_i^x S_j^x + S_i^y S_j^y - \left(S_i^z S_j^z - \frac{1}{4} n_i n_j \right), \end{aligned} \quad (\text{S12})$$

where $\sigma \in \{+1, -1\}$ for $\{\uparrow, \downarrow\}$ respectively when serving as a coefficient. Therefore, the effective Hamiltonian of the spinful hard-core Bose-Hubbard model at $U \gg t$ up to the second order is

$$H_{\text{eff}} = \mathcal{P}_s (H_t + H_J^-) \mathcal{P}_s, \quad (\text{S13})$$

where

$$\begin{aligned} H_t &= -t \sum_{\langle ij \rangle \sigma} \left(B_{i\sigma}^\dagger B_{j\sigma} + \text{h.c.} \right), \\ H_J^- &= J \sum_{\langle ij \rangle} \left(-S_i^x S_j^x - S_i^y S_j^y + S_i^z S_j^z - \frac{1}{4} n_i n_j \right). \end{aligned} \quad (\text{S14})$$

This effective Hamiltonian is quite similar to the bosonic t - J model except that the in-plane (S^x, S^y) spin-exchange is ferromagnetic (FM). The root cause is that exchanging two fermions of different spin states yields a negative sign while that for spinful hard-core bosons does not. This is a significant difference compared to the fermionic case where the effective model of the Fermi-Hubbard model at $U \gg t$ is just the fermionic t - J model. Note that the spin-exchange coupling along S^z in Eq. (S14) is still antiferromagnetic, in line with the common argument about the Hubbard model, i.e., the nearest-neighboring (NN) spins tend to be antiparallel because NN parallel spins cannot gain kinetic energy from the second-order virtual hopping process due to the Pauli exclusion principle or hard-core property while NN antiparallel spins can. Note that if the following identity is applied

$$S_i^z S_j^z - \frac{1}{4} n_i n_j = \frac{1}{4} \sum_{\sigma\sigma'} (\sigma\sigma' - 1) n_{i\sigma} n_{j\sigma'} = \frac{1}{4} \sum_{\sigma\sigma'} (-2\delta_{\sigma, -\sigma'}) n_{i\sigma} n_{j\sigma'} = -\frac{1}{2} \sum_{\sigma} n_{i\sigma} n_{j, -\sigma}, \quad (\text{S15})$$

the anisotropic bosonic t - J model in Eq. (S14) will have exactly the same form as in Ref. [68–70].

We remark that the term H_J^- in Eq. (S14) explicitly breaks the spin-SU(2) rotation symmetry. The reason can be actually traced back to the fact that the hopping term in the original spinful hard-core Bose-Hubbard model in Eq. (S1) has already broken the spin-SU(2) rotation symmetry implicitly as the on-site fermion sign between different \uparrow - or \downarrow -spins has been removed and replaced by the “artificial” spinful hard-core boson statistics. Moreover, as we will discuss in the next section, the effective model in Eq. (S14) is sign-problem-free or say sign-free, consistent with the fact that the original spinful hard-core Bose-Hubbard model in Eq. (S1) is also a sign-free model.

From above one can see that the effective model of the spinful hard-core Bose-Hubbard model at half-filling is not the Heisenberg model anymore. But it is possible to recover the Heisenberg limit by introducing an on-site unitary (phase) transformation on bipartite lattices like square lattices that changes the sign of the in-plane spin-exchange interaction, i.e., the so-called Marshall transformation

$$U_{\text{Ms}} = (-1)^{N_A^\downarrow} = \prod_{i \in A} (-1)^{n_{i\downarrow}} = \prod_{i \in A} e^{-iS_i^z \pi} e^{i\pi/2}, \quad (\text{S16})$$

where N_A^\downarrow denotes the total number of \downarrow -spins on sublattice A . The choices of A or B sublattice and \downarrow - or \uparrow -spins in this transformation are arbitrary. Here we just choose to count \downarrow -spins on sublattice A . This Marshall transformation can be seen as a U(1) gauge transformation via the mapping between spins and hard-core bosons.

For a real-space Fock state, here referring to a product state composed of single-site spin-up, spin-down, and unoccupied states $\{|\uparrow\rangle, |\downarrow\rangle, |0\rangle\}$ (a hole-spin configuration), if the state on site i of sublattice A is $|\downarrow\rangle$, U_{Ms} will attach

a negative sign to the state $|\downarrow\rangle \rightarrow -|\downarrow\rangle$. The transformed basis is called the ‘‘Marshall basis’’. In such a way, S_i^x and S_i^y on sublattice A can obtain a negative sign while S_i^z on sublattice A keeps unchanged, i.e.,

$$U_{\text{Ms}}^\dagger S_i^x U_{\text{Ms}} = -S_i^x, \quad U_{\text{Ms}}^\dagger S_i^y U_{\text{Ms}} = -S_i^y, \quad U_{\text{Ms}}^\dagger S_i^z U_{\text{Ms}} = S_i^z, \quad i \in A. \quad (\text{S17})$$

Hence, the transformed spin-exchange term becomes isotropically antiferromagnetic (AFM). At the same time, the hopping term should also change under this unitary transformation according to

$$U_{\text{Ms}}^\dagger B_{i\sigma} U_{\text{Ms}} = \sigma B_{i\sigma}, \quad U_{\text{Ms}}^\dagger B_{i\sigma}^\dagger U_{\text{Ms}} = \sigma B_{i\sigma}^\dagger, \quad i \in A. \quad (\text{S18})$$

Namely, a spin-dependent sign σ will be attached to the NN hopping term. Assuming i is an odd number for each $i \in A$, the expression above can be simplified to

$$U_{\text{Ms}}^\dagger B_{i\sigma} U_{\text{Ms}} = \sigma^i B_{i\sigma}. \quad (\text{S19})$$

Therefore, the transformed effective Hamiltonian becomes exactly the bosonic σt - J model

$$H_{\sigma t-J} = U_{\text{Ms}}^\dagger H_{\text{eff}} U_{\text{Ms}} = \mathcal{P}_s (H_{\sigma t} + H_J) \mathcal{P}_s, \quad (\text{S20})$$

where

$$\begin{aligned} H_{\sigma t} &= -t \sum_{\langle ij \rangle \sigma} \sigma \left(B_{i\sigma}^\dagger B_{j\sigma} + \text{h.c.} \right), \\ H_J &= J \sum_{\langle ij \rangle} \left(\mathbf{S}_i \cdot \mathbf{S}_j - \frac{1}{4} n_i n_j \right). \end{aligned} \quad (\text{S21})$$

Remember that $\sigma \in \{+1, -1\}$ for $\{\uparrow, \downarrow\}$ respectively when serving as a coefficient. In summary, in the limit of $U \gg t$, the spinful hard-core Bose-Hubbard model should effectively have the same nature as the bosonic σt - J model, up to the Marshall transformation that maps in-plane ferromagnetism to in-plane antiferromagnetism.

II. Quantum frustration analysis

In this section, we analyze the quantum frustrations or say the sign structures of the models mentioned in the main text based on explicit power series expansions of the partition functions. Here the term ‘‘quantum frustration’’ or ‘‘sign structure’’ refers to the form of the sign (phase) factor in the path-integral-type summation of the partition function.

A. Bosonic t - J model

We first analyze the sign structure of the bosonic t - J model on bipartite lattices. After the Marshall transformation in Eq. (S16), the Hamiltonian of the bosonic t - J model can be rewritten as

$$\begin{aligned} U_{\text{Ms}}^\dagger H_{t-J} U_{\text{Ms}} &= H_{\sigma t} + H_J^{(-)} \\ &= -t (T_{o\uparrow} - T_{o\downarrow}) - \frac{J}{2} (T_{\uparrow\downarrow} + V_{\uparrow\downarrow}), \end{aligned} \quad (\text{S22})$$

where

$$T_{o\sigma} = \sum_{\langle ij \rangle} B_{i\sigma}^\dagger B_{j\sigma} + \text{h.c.}, \quad (\text{S23})$$

$$T_{\uparrow\downarrow} = \sum_{\langle ij \rangle} B_{i\uparrow}^\dagger B_{i\downarrow} B_{j\downarrow}^\dagger B_{j\uparrow} + \text{h.c.}, \quad (\text{S24})$$

$$V_{\uparrow\downarrow} = \sum_{\langle ij \rangle} (n_{i\uparrow} n_{j\downarrow} + n_{i\downarrow} n_{j\uparrow}). \quad (\text{S25})$$

Here we omit to write down the no-double-occupancy projector \mathcal{P}_s explicitly and absorb it into each single-particle operator for simplicity (the same below). $T_{o\sigma}$ describes the NN exchange process of holes and σ -spins, $T_{\uparrow\downarrow}$ describes

the NN exchange process of \uparrow -spins and \downarrow -spins, and $V_{\uparrow\downarrow}$ describes the potential energy of NN antiparallel spins. The series expansion of the corresponding partition function up to infinite orders reads [13]

$$\begin{aligned} Z_{t-J} &= \text{Tr} e^{-\beta H_{t-J}} = \text{Tr} e^{-\beta U_{\text{Ms}}^\dagger H_{t-J} U_{\text{Ms}}} = \text{Tr} \sum_{n=0}^{\infty} \frac{\beta^n}{n!} \left(-U_{\text{Ms}}^\dagger H_{t-J} U_{\text{Ms}} \right)^n \\ &= \sum_{n=0}^{\infty} \frac{\beta^n}{n!} \text{Tr} \left[\sum \cdots (tT_{o\uparrow}) \cdots \left(\frac{J}{2} T_{\uparrow\downarrow} \right) \cdots (-tT_{o\downarrow}) \cdots \left(\frac{J}{2} V_{\uparrow\downarrow} \right) \cdots \right]_n \\ &= \sum_{n=0}^{\infty} \frac{\beta^n}{n!} \text{Tr} \left[\sum (-1)^{N_{\downarrow}^h} \cdots (tT_{o\uparrow}) \cdots \left(\frac{J}{2} T_{\uparrow\downarrow} \right) \cdots (tT_{o\downarrow}) \cdots \left(\frac{J}{2} V_{\uparrow\downarrow} \right) \cdots \right]_n. \end{aligned} \quad (\text{S26})$$

The formal notation $[\sum \cdots]_n$ indicates the summation over all length- n process combination of $T_{o\uparrow}$, $T_{o\downarrow}$, $T_{\uparrow\downarrow}$, and $V_{\uparrow\downarrow}$. Here N_{\downarrow}^h denotes the total number of NN exchanges between holes and \downarrow -spins $T_{o\downarrow}$. We remark that the remaining part in Eq. (S26) except $(-1)^{N_{\downarrow}^h}$ is always non-negative because each matrix element in $T_{o\uparrow}$, $T_{o\downarrow}$, $T_{\uparrow\downarrow}$, and $V_{\uparrow\downarrow}$ is non-negative.

By further expanding $T_{o\uparrow}$, $T_{o\downarrow}$, $T_{\uparrow\downarrow}$, and $V_{\uparrow\downarrow}$ into elementary local terms and writing the trace as the sum of expectations over the complete Fock basis (or equivalently by inserting complete bases between each ‘‘time slice’’), the partition function can be expressed by a huge summation of real numbers with each number indexed by a discrete evolution of hole-spin configurations, where in each step, one of the four events $T_{o\uparrow}$, $T_{o\downarrow}$, $T_{\uparrow\downarrow}$, and $V_{\uparrow\downarrow}$ occurs at a certain link $\langle ij \rangle$. Note that due to the trace operation, the initial and final hole-spin configurations in the evolution should be the same, so in each possible evolution path C , the motion of holes and spins must form closed loops. Namely, the partition function can be expressed by a summation that runs over all possible closed evolution paths C , i.e.,

$$Z_{t-J} = \sum_C \tau_C W_{t-J}[C], \quad (\text{S27})$$

where

$$\tau_C = (-1)^{N_{\downarrow}^h}, \quad (\text{S28})$$

is the sign structure of the bosonic t - J model and $W_{t-J}[C] \geq 0$ denotes a non-negative weight corresponding to the evolution path C with its explicit form omitted. Note that the summation over evolution length n in Eq. (S26) has been included in the summation over evolution path C in Eq. (S27). Importantly, we find that the sign structure $(-1)^{N_{\downarrow}^h}$ can be interpreted as mutual statistics of holes and \downarrow -spins. Namely, an exchange of a hole and a \downarrow -spin will give rise to a minus sign during the evolution determined by the bosonic t - J model.

Here we elaborate on why we focus on the sign structure after applying the Marshall transformation. Of course, one can write down the sign structure without applying the Marshall transformation, which is just $(-1)^{N_{\uparrow\downarrow}}$ with $N_{\uparrow\downarrow}$ denoting the number of NN exchanges between \uparrow -spins and \downarrow -spins $T_{\uparrow\downarrow}$. This can be seen as a type of ‘‘fermion’’ statistics between \uparrow -spins and \downarrow -spins. It is equivalent to Eq. (S28) because phase transformations cannot change the overall sign of an evolution loop. However, at half-filling where the model is reduced to the Heisenberg model in which the Marshall transformation is first introduced, the sign $(-1)^{N_{\downarrow}^h}$ naturally disappears due to the absence of holes while $(-1)^{N_{\uparrow\downarrow}}$ is still present, in spite that eventually $(-1)^{N_{\uparrow\downarrow}}$ will cancel with each other due to the periodic boundary condition along the time direction. This implies that at low doping levels, it is natural and beneficial to exploit the sign structure $(-1)^{N_{\downarrow}^h}$ which treats doped holes as an essential object. Physically, at half-filling, treating spinons as bosons can naturally and correctly give rise to AFM long-range order via the Schwinger boson mean-field theory. This suggests that one shall continuously treat spinons as bosons at least when slightly deviating from half-filling, which also justifies the fundamental role of the sign structure $(-1)^{N_{\downarrow}^h}$ at low doping levels.

B. Bosonic σt - J model

For the bosonic σt - J model in Eq. (S20), an extra spin-dependent sign σ is attached to the NN hopping term compared to the bosonic t - J model. As a result, after the Marshall transformation, this spin-dependent sign can exactly cancel the negative sign in front of $T_{o\downarrow}$ that arises from the transformation, i.e.,

$$U_{\text{Ms}}^\dagger H_{\sigma t-J} U_{\text{Ms}} = -t(T_{o\uparrow} + T_{o\downarrow}) - \frac{J}{2}(T_{\uparrow\downarrow} + V_{\uparrow\downarrow}). \quad (\text{S29})$$

Similar to Eq.(S26), one can perform series expansions for the bosonic σt - J model and find that everything is the same as the expression of the bosonic t - J model except that the sign structure $(-1)^{N\downarrow}$ disappears (or say simply becomes 1). The non-negative weight $W[C]$ corresponding to each evolution path C is exactly the same as that of the bosonic t - J model. That is to say, the bosonic σt - J model is a “sign-free” model, i.e., it can be efficiently simulated by quantum Monte Carlo methods without any sign (phase) problem, such as the stochastic series expansion (SSE) method. This can be easily seen from Eq. (S29) because each matrix element of $(-U_{\text{Ms}}^\dagger H_{\sigma t-J} U_{\text{Ms}})$ under the real-space Fock basis is non-negative.

C. Spinful hard-core Bose-Hubbard model

Similar to the derivation above, it is straightforward to prove that the spinful hard-core Bose-Hubbard model defined in Eq.(S1) is also sign-free because the matrix elements of the minus hopping term $(-H_t)$ (off-diagonal) are all non-negative, i.e., equal t or 0, and the matrix elements of the minus on-site Hubbard term $(-H_U)$ (diagonal) can also be shifted to non-negative values by adding a constant to each local term to make $(-U)$ or 0 shifted to 0 or U . Note that one can always add a constant to the Hamiltonian without changing the expectation values of any other observables and add it back when calculating the energy. The sign-free property of the spinful hard-core Bose-Hubbard model is consistent with the fact that its effective model in the limit of $U \gg t$, i.e., the bosonic σt - J model, is also sign-free.

D. Relation with the continuous Berry phase

In the main text, we mention that the frustration phase τ_C can be seen as a generalized discrete version of the Berry phase action in the continuous path integral formalism of conventional models, in the sense that it is an “adiabatic” phase independent of the evolution speed, in contrast to the dynamical phase stemming from the exponentiated imaginary unit i in the real-time evolution. Here we provide another perspective to justify the close relationship between the frustration phase and the conventional continuous Berry phase.

For a parametrized quantum state $|\alpha(R)\rangle$, the conventional continuous Berry phase takes the form of

$$\gamma_C = i \oint_C \langle \alpha(R) | \nabla_R | \alpha(R) \rangle \cdot dR, \quad (\text{S30})$$

where C represents a closed path in the parameter space. If one replaces the continuous path with a discrete series of quantum states $\{|\alpha_0\rangle, |\alpha_1\rangle, \dots, |\alpha_{n-1}\rangle\}$, the Berry phase becomes

$$\gamma_C = \text{Im} \ln \langle \alpha_{n-1} | \alpha_{n-2} \rangle \cdots \langle \alpha_2 | \alpha_1 \rangle \langle \alpha_1 | \alpha_0 \rangle. \quad (\text{S31})$$

That is to say, γ_C counts the phase differences between each pair of adjacent states. On the other hand, as mentioned in the main text, the frustration phase takes the form of

$$\tau_C = \text{Im} \ln \langle \alpha_{n-1} | (-H) | \alpha_{n-2} \rangle \cdots \langle \alpha_2 | (-H) | \alpha_1 \rangle \langle \alpha_1 | (-H) | \alpha_0 \rangle. \quad (\text{S32})$$

Hence, the frustration phase can be seen exactly as a Berry phase if one absorbs the operator $(-H)$ into the original series of quantum states. We emphasize that the discreteness stems from the expansion scheme where a discrete complete basis is inserted. It is possible to realize a continuous form of the frustration phase if some appropriate continuous complete basis is applied like in the spin coherent state path integral.

III. Analysis on the phase of pairing order parameter

A. Pairing in bosonic systems

In this section, we discuss the basic properties of possible pairing states allowed in bosonic models. The generic two-body wavefunction of a “bosonic Cooper pair” with the decoupled spatial and spin sectors can be expressed as

$$\psi(R, r; \sigma_1, \sigma_2) = \phi(R, r) \chi(\sigma_1, \sigma_2), \quad (\text{S33})$$

where $\phi(R, r)$ and $\chi(\sigma_1, \sigma_2)$ represents the spatial and spin sectors. R denotes the center-of-mass position and r denotes the relative position. It is important to note that the exchange of two bosons, i.e., $r \rightarrow -r$ and $\sigma_1 \rightarrow \sigma_2$,

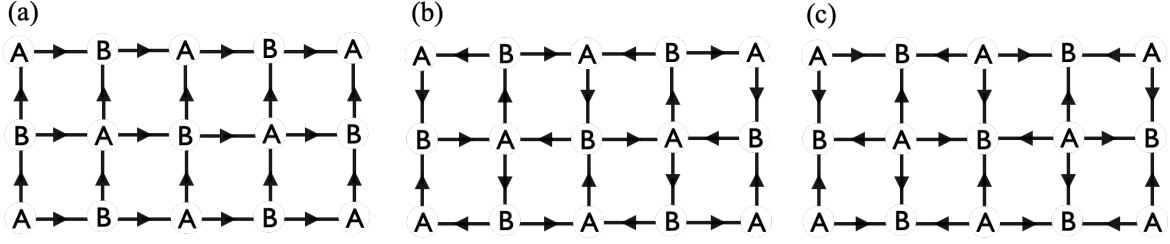


FIG. S1. Three possible nearest-neighbor (NN) spin-singlet pairing sign patterns in spin-1/2 hard-core bosonic systems. The labels A and B denote the two sublattices of a square lattice. The arrow direction indicates the sign of the NN singlet pairing order parameter $\langle \Delta_{i\alpha} \rangle$. If α takes the same direction as the arrow, $\langle \Delta_{i\alpha} \rangle$ is positive, and vice versa.

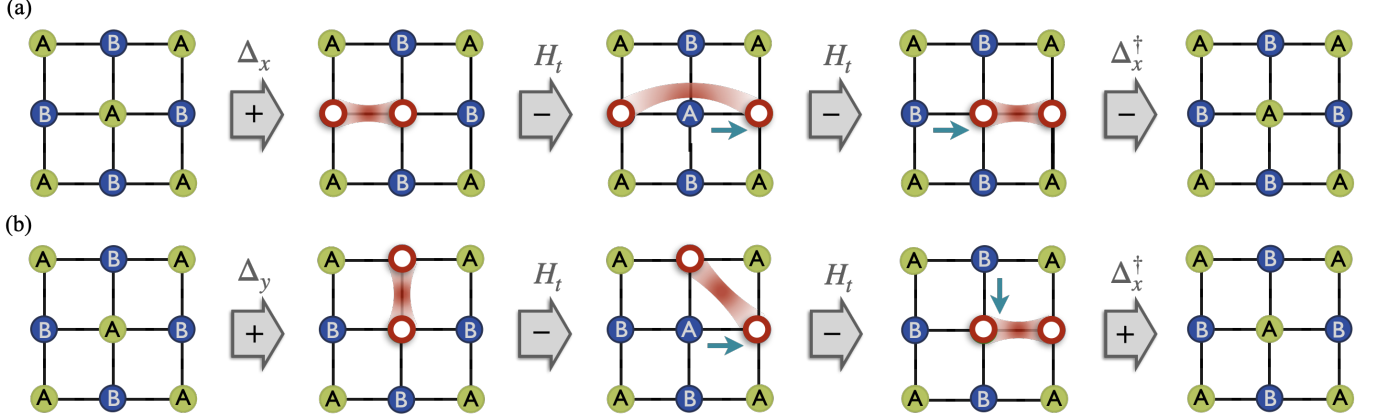


FIG. S2. Schematic illustration of two representative imaginary-time evolution loops for the singlet pair-pair correlation under the Marshall basis. The labels A and B denote the two sublattices of a square lattice. The green and blue circles represent spins in $|\uparrow\rangle$ and $|\downarrow\rangle$. The red hollow circles represent holes $|0\rangle$. The positive and negative signs in the grey arrow indicate the sign caused by the corresponding process. (a) A representative hopping procedure for a hole pair in the correlation function $\langle \Delta_{i\hat{x}} \Delta_{i+\hat{x}}^\dagger \rangle$. The negative sign created by H_t arises from the matrix elements under the Marshall basis as in Eq. (S28). (b) A representative hopping procedure for a hole pair in the correlation function $\langle \Delta_{ij} \Delta_{i\hat{x}}^\dagger \rangle$. Here we use $\langle \Delta_{j\beta} \Delta_{i\alpha}^\dagger \rangle$ instead of $\langle \Delta_{i\alpha}^\dagger \Delta_{j\beta} \rangle$ just for the simplicity of illustration.

will not result in an additional minus sign, which differs from conventional fermionic systems. Therefore, if the spin sector is in an anti-symmetric singlet state $(|\uparrow\downarrow\rangle - |\downarrow\uparrow\rangle)/\sqrt{2}$, the corresponding spatial sector should exhibit odd parity $\phi(R, r) = -\phi(R, -r)$ leading to a p -wave symmetry, etc.

For a spatially uniform spin-singlet pairing order, as shown in Fig. S1(a), it will naturally exhibit a p -wave rotational symmetry, i.e., a π rotation yields a negative sign, because the bosonic spin-singlet is directed, i.e., $\Delta_{i\alpha} = -\Delta_{i+\alpha, -\alpha}$ with $\Delta_{i\alpha} = \sum_{\sigma} \sigma B_{i,\sigma} B_{i+\alpha, -\sigma} / \sqrt{2}$, in contrast to the fermionic case. Then we consider a spatially modulated singlet pairing order with a (π, π) wavevector, i.e., it has staggered oscillations in both spatial directions. Figs. S1(b) and (c) show two different possible nearest-neighbor (NN) spin-singlet pairing patterns under this condition, which can be characterized by the sign factors $(-1)^{i+\alpha_x}$ and $(-1)^{i+\alpha}$, respectively. Here the notation $(-1)^i$ takes (-1) if $i \in A$ and takes $(+1)$ if $i \in B$, which can also be written as $(-1)^{x+y}$ with $i = (x, y)$ if the origin point belongs to sublattice B. α is the link vector in $\Delta_{i\alpha}$ and α_x represents its component along the \hat{x} direction. These two NN pairing sign patterns exhibit a “local” d -wave symmetry and a “local” s -wave symmetry respectively, in the sense that the four NN links around a single site follow the corresponding sign change rule. The DMRG results in this paper show that the actual pattern of the AFM-PDW phase in the bosonic t - J model is Fig. S1(c).

B. Pairing phase from the Marshall sign and constructive interference

Here we provide a detailed argument to explain the origin of the (π, π) -PDW observed in DMRG simulations as depicted in Fig. 1(b). Under the Marshall basis defined by Eq. (S16), the singlet pair-pair correlation function can be

expressed as

$$\begin{aligned}
\langle \Delta_{i\alpha}^\dagger \Delta_{j\beta} \rangle &= \frac{1}{Z} \text{Tr} \left(e^{-\beta H} \Delta_{i\alpha}^\dagger \Delta_{j\beta} \right) = \frac{1}{Z} \text{Tr} \left(e^{-\beta U_{\text{Ms}}} H U_{\text{Ms}}^\dagger U_{\text{Ms}} \Delta_{i\alpha}^\dagger \Delta_{j\beta} U_{\text{Ms}}^\dagger \right) \\
&= \frac{1}{Z} \text{Tr} \left(e^{-\beta U_{\text{Ms}}} H U_{\text{Ms}}^\dagger (-1)^{i+\alpha} \Delta_{i\alpha}^{t\dagger} (-1)^{j+\beta} \Delta_{j\beta}^t \right) \\
&= (-1)^{(j-i)+(\beta-\alpha)} \frac{1}{Z} \text{Tr} \left(\Delta_{j\beta}^t e^{-\beta U_{\text{Ms}}} H U_{\text{Ms}}^\dagger \Delta_{i\alpha}^{t\dagger} \right),
\end{aligned} \tag{S34}$$

where $\Delta_{i\alpha}^t = \sum_\sigma B_{i\sigma} B_{i+\alpha, \sigma} / \sqrt{2}$ is the $S^z = 0$ spin-triplet pair annihilation operator. Similar to the series expansion of the partition function in Eq. (S26), one can expand the pair-pair correlation function as

$$\langle \Delta_{i\alpha}^\dagger \Delta_{j\beta} \rangle = (-1)^{(j-i)+(\beta-\alpha)} \frac{1}{Z} \sum_{n=0}^{\infty} \frac{\beta^n}{n!} \text{Tr} \left[\sum \Delta_{j\beta}^t \cdots (tT_{o\uparrow}) \cdots \left(\frac{J}{2} T_{\uparrow\downarrow} \right) \cdots (-tT_{o\downarrow}) \cdots \left(\frac{J}{2} V_{\uparrow\downarrow} \right) \cdots \Delta_{i\alpha}^{t\dagger} \right]_n. \tag{S35}$$

Except the sign factor $(-1)^{(j-i)+(\beta-\alpha)}$ and the exchange of holes and \downarrow spins ($-tT_{o\downarrow}$), the remaining parts are positive-definite, including $\Delta_{j\beta}^t$ and $\Delta_{i\alpha}^{t\dagger}$. In general, one cannot determine the sign of the huge summation in Eq. (S35) due to the existence of the negative ingredient ($-tT_{o\downarrow}$). However, we know there exists a leading positive contribution from the ‘‘in-tandem’’ propagation of hole pairs, which always includes an even number of ($-tT_{o\downarrow}$) resulting in an extensive summation of positive weights (‘‘constructive interference’’). If this contribution is dominant over the others (which is very likely as the other parts may cancel each other out due to the phase fluctuation), then the huge summation in Eq. (S35) should be positive. Therefore, the overall sign of the NN singlet pair-pair correlation $\langle \Delta_{i\alpha}^\dagger \Delta_{j\beta} \rangle$ should be just determined by the factor $(-1)^{(j-i)+(\beta-\alpha)}$ resulting from the Marshall sign. After fixing one of the pair operators at $j + \beta = 0$ without loss of generality, the phase of the NN singlet pairing order parameter is in the form $(-1)^{i+\alpha}$, i.e., the one depicted in Fig. S1(c), which is consistent with the DMRG results shown in the main text.

In summary, the strings of \mathbb{Z}_2 phases caused by the hopping of two holes under the Marshall basis can be canceled with each other by forming a tightly bound pair, resulting in constructive interference, so that the only remaining phase of the pairing order parameter comes from the transformed pair operators themselves, i.e., the Marshall sign. We further illustrate two representative evolution paths in Fig. S2 as examples for clarity.

In addition, the above argument is based on the assumption that the ground state is not an FM state, i.e., the weights that mainly involve globally polarized spins are not dominant in the summation in Eq. (S35), where the sign factor $(-1)^{N_\downarrow} \rightarrow 1$ become trivial and no destructive interference occurs in the single-particle propagation. Otherwise, the contribution where holes form pairs would become sub-leading and no pairing could be observed in the resulting ground state.

IV. Parton construction of the bosonic σt - J model

A. Mean-field scheme

In this section, we present more details of the parton construction approach used to describe the bosonic σt - J model. We decompose the original boson operator subject to the no-double-occupancy constraint into

$$B_i = b_{i\sigma} h_i^\dagger \tag{S36}$$

where $b_{i\sigma}$ denotes the bosonic spinon with spin σ and h_i^\dagger denotes the bosonic holon. Then, the bosonic σt - J model in Eq. (S20) can be expressed as follows

$$H_{\sigma t-J} = t \sum_{\langle ij \rangle, \sigma} \sigma \hat{\chi}_{ij, \sigma} \hat{\kappa}_{ij}^\dagger + \text{H.c.} - \frac{J}{2} \sum_{ij} \hat{\Delta}_{ij}^\dagger \hat{\Delta}_{ij}, \tag{S37}$$

where

$$\hat{\kappa}_{ij} = h_i^\dagger h_j, \quad \hat{\chi}_{ij, \sigma} = b_{i, \alpha}^\dagger b_{j, \sigma}, \quad \hat{\Delta}_{ij} = \sum_{\sigma} \sigma b_{i, \sigma} b_{j, -\sigma}, \tag{S38}$$

with the relation

$$\hat{\kappa}_{ji} = \hat{\kappa}_{ij}^\dagger, \quad \hat{\chi}_{ji, \sigma} = \hat{\chi}_{ij, \sigma}^\dagger, \quad \hat{\Delta}_{ji} = -\hat{\Delta}_{ij}. \tag{S39}$$

Based on the mean-field ansatz $\hat{\kappa}_{ij} = i\kappa$, $\hat{\chi}_{ij,\sigma} = i\sigma\chi$, and $\hat{\Delta}_{ij} = i\Delta$, the Hamiltonian (S37) at the mean-field level can be decomposed into the holon part H_h and the spinon part H_b , with the form

$$H_h = -4t\chi \sum_k \mathcal{E}_k h_k^\dagger h_k - \mu \sum_k \left(h_k^\dagger h_k - \delta \right), \quad (\text{S40})$$

and

$$\begin{aligned} H_b = & -2t\kappa \sum_{k,\sigma} \sigma \mathcal{E}_k b_{k,\sigma}^\dagger b_{k,\sigma} + J\Delta \sum_k \mathcal{E}_k (b_{-k,\downarrow} b_{k,\uparrow} + \text{H.c.}) \\ & + J\Delta^2 N - 8tN\chi\kappa + \lambda \sum_k \left(\sum_\sigma b_{k,\sigma}^\dagger b_{k,\sigma} - 1 + \delta \right), \end{aligned} \quad (\text{S41})$$

where $\mathcal{E}_k = \sin k_x + \sin k_y$, and κ , χ , and Δ are all chosen to be real numbers. Here, μ and λ are the chemical potentials controlling the holon number δ and spinon number $1 - \delta$, respectively. From Eq. (S40), the dispersion for the holon is given by

$$E_k^h = -4t\chi\mathcal{E}_k - \mu. \quad (\text{S42})$$

Similarly, from Eq. (S41), by introducing the following Bogoliubov transformation, we obtain the spinon dispersion

$$E_k^b = \sqrt{\lambda_k^2 - \Delta_k^2}, \quad (\text{S43})$$

where $\lambda_k = \lambda - 2t\kappa\mathcal{E}_k$ and $\Delta_k = J\Delta\mathcal{E}_k$. The values of the mean-field ansatz and chemical potentials can be determined via self-consistent calculations as follows:

$$\begin{aligned} \frac{\partial F}{\partial \lambda} = 0 & \implies \frac{1}{N} \sum_k \frac{(\lambda - 2t\kappa\mathcal{E}_k)}{E_k^b} \coth\left(\frac{1}{2}\beta E_k^b\right) + (-2 + \delta) = 0, \\ \frac{\partial F}{\partial \mu} = 0 & \implies \frac{1}{N} \sum_k \frac{1}{e^{\beta E_k^h} - 1} - \delta = 0, \\ \frac{\partial F}{\partial \kappa} = 0 & \implies \frac{1}{N} \sum_k \frac{\mathcal{E}_k (\lambda - 2t\kappa\mathcal{E}_k)}{E_k^b} \coth\left(\frac{1}{2}\beta E_k^b\right) + 4\chi = 0, \\ \frac{\partial F}{\partial \chi} = 0 & \implies \frac{1}{N} \sum_k \frac{\mathcal{E}_k}{e^{\beta E_k^h} - 1} + 2\kappa = 0, \\ \frac{\partial F}{\partial \Delta} = 0 & \implies 2 - \frac{1}{N} \sum_k \frac{J\mathcal{E}_k^2}{E_k^b} \coth\left(\frac{1}{2}\beta E_k^b\right) = 0. \end{aligned} \quad (\text{S44})$$

Based on the calculated mean-field parameters at $T \rightarrow 0$, the holon dispersion Eq. (S42) is shown in Fig. S3(a), indicating that the band bottom is located at the momentum $(\pi/2, \pi/2)$. Similarly, the spinon dispersion Eq. (S43) is shown in Fig. S3(b), exhibiting low-lying modes near the momentum $(-\pi/2, -\pi/2)$. The temperature dependence of the excitation gap for holons E_{\min}^h and for spinons E_{\min}^b are shown in Figs. S3(c) and (d), respectively. These figures show that both spinons and holons tend to be gapless in the zero temperature limit, indicating that both tend to undergo Bose-Einstein condensation as the temperature approaches zero.

In addition, spinons with opposite spin directions occupy band minima at opposite momenta: the \uparrow -spinon is located at $(-\pi/2, -\pi/2)$ while the \downarrow -spinon is at $(\pi/2, \pi/2)$, as directly obtained from the corresponding Green's functions in Eqs. (S45)-(S46). When combined with the condensation of holons at $(\pi/2, \pi/2)$, this results in actual bosons with \uparrow -spin condensing at $(0, 0)$ momentum, while \downarrow -spin condenses at (π, π) momentum. This finding is consistent with the σ^r factor observed in the DMRG results [see Fig. 4(a)].

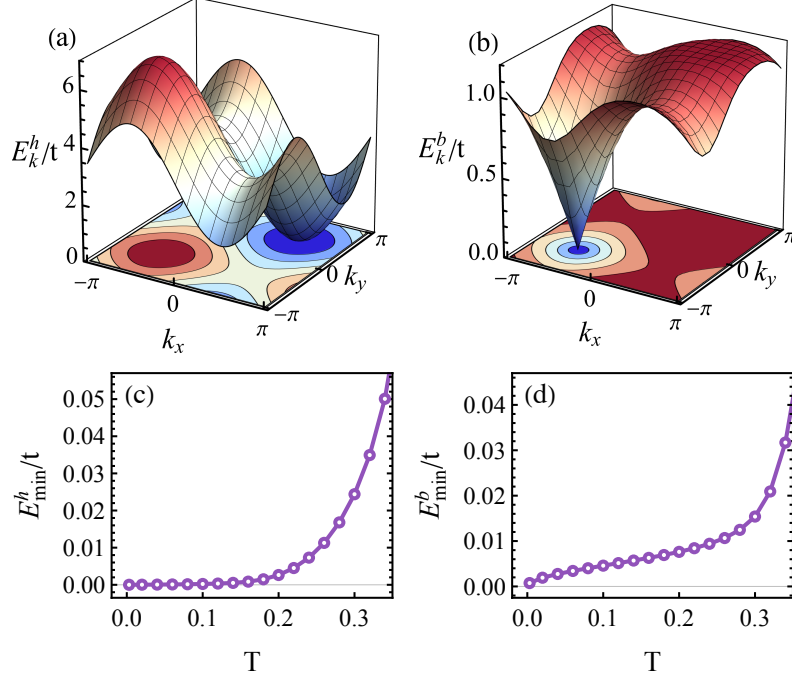


FIG. S3. With parameters $J = t/3$ and doping density $\delta = 1/12$. Dispersions for holons E_k^h and spinons E_k^b are shown in (a) and (b), respectively. The lowest excitation energy gaps for holons and spinons are shown in (c) and (d), respectively.

B. Spin response

According to Eq. (S41), the normal and anomalous Green's functions of spinons are given by:

$$G_{\uparrow\uparrow}(k, \omega) = -\langle b_{k\uparrow}(\omega)b_{k\uparrow}^\dagger(\omega) \rangle = \frac{\lambda_k + \omega}{\omega^2 - (E_k^b)^2}, \quad (\text{S45})$$

$$G_{\downarrow\downarrow}(k, \omega) = -\langle b_{k\downarrow}(\omega)b_{k\downarrow}^\dagger(\omega) \rangle = \frac{\lambda_{-k} + \omega}{\omega^2 - (E_{-k}^b)^2}, \quad (\text{S46})$$

$$G_{*\downarrow\downarrow}(-k, -\omega) = -\langle b_{-k\downarrow}^\dagger(-\omega)b_{-k\downarrow}(-\omega) \rangle = \frac{\lambda_k - \omega}{\omega^2 - (E_k^b)^2}, \quad (\text{S47})$$

$$G_{*\uparrow\uparrow}(-k, -\omega) = -\langle b_{-k\uparrow}^\dagger(-\omega)b_{-k\uparrow}(\omega) \rangle = \frac{\lambda_{-k} - \omega}{\omega^2 - (E_{-k}^b)^2}, \quad (\text{S48})$$

$$F_{\uparrow\downarrow}(k, \omega) = -\langle b_{k\uparrow}(\omega)b_{-k\downarrow}(-\omega) \rangle = -\frac{\Delta_k}{\omega^2 - (E_k^b)^2}, \quad (\text{S49})$$

$$F_{\downarrow\uparrow}(k, \omega) = -\langle b_{k\downarrow}(\omega)b_{-k\uparrow}(-\omega) \rangle = \frac{\Delta_k}{\omega^2 - (E_{-k}^b)^2}, \quad (\text{S50})$$

$$F_{*\downarrow\uparrow}(-k, -\omega) = -\langle b_{-k\downarrow}^\dagger(-\omega)b_{k\uparrow}^\dagger(\omega) \rangle = -\frac{\Delta_k}{\omega^2 - (E_k^b)^2}, \quad (\text{S51})$$

$$F_{*\uparrow\downarrow}(-k, -\omega) = -\langle b_{-k\uparrow}^\dagger(-\omega)b_{k\downarrow}^\dagger(\omega) \rangle = \frac{\Delta_k}{\omega^2 - (E_{-k}^b)^2}. \quad (\text{S52})$$

Then, by the relation $S_i^z = \frac{1}{2} \sum_{\sigma} \sigma b_{i\sigma}^\dagger b_{i\sigma}$, the Matsubara spin-spin correlation function along the z -spin direction can be expressed as

$$\begin{aligned} \chi^{zz}(i, j, \tau) &\equiv \langle \hat{T} S_j^z(\tau) S_i^z(0) \rangle_0 = \frac{1}{4} \sum_{\sigma, \sigma'} \sigma \sigma' \langle \hat{T} b_{j, \sigma}^\dagger(\tau) b_{j, \sigma}(\tau) b_{i, \sigma'}^\dagger(0) b_{i, \sigma'}(0) \rangle_0 \\ &= \frac{1}{4} [G_{*\uparrow\uparrow}(r, \tau) G_{\uparrow\uparrow}(r, \tau) + G_{*\downarrow\downarrow}(r, \tau) G_{\downarrow\downarrow}(r, \tau) - F_{*\downarrow\uparrow}(r, \tau) F_{\uparrow\downarrow}(r, \tau) - F_{*\uparrow\downarrow}(r, \tau) F_{\downarrow\uparrow}(r, \tau)], \end{aligned} \quad (\text{S53})$$

where $\langle \cdot \rangle_0$ denotes the expectation value under the mean-field state, and Wick's theorem is applied in the last line. Then, the spin correlation function in momentum and frequency space at $T = 0$ can be expressed as

$$\begin{aligned} \chi^{zz}(\mathbf{k}, i\omega_n) &= \int_0^\beta d\tau \sum_i e^{-ik \cdot r} e^{i\omega_n \tau} \chi^{zz}(r, \tau) \\ &= -\frac{1}{16N} \sum_q \frac{\left(E_q^b E_{k+q}^b - \lambda_q \lambda_{k+q} \right) + i\omega_n \left(-E_{k+q}^b \lambda_q + E_q^b \lambda_{k+q} \right) / \left(E_q^b + E_{k+q}^b \right) + \Delta_q \Delta_{k+q}}{E_q^b E_{k+q}^b} \\ &\quad \times \left(-\frac{1}{i\omega_n - E_q^b - E_{k+q}^b} + \frac{1}{i\omega_n + E_q^b + E_{k+q}^b} \right) + (k \leftrightarrow -k). \end{aligned} \quad (\text{S54})$$

Similarly, by using the relation $S_i^\pm = \frac{1}{2}(S_i^x \pm iS_i^y)$, the Matsubara spin-spin correlation function along the x - y plane can be expressed as

$$\begin{aligned} \chi^{+-}(i, j, \tau) &\equiv \left\langle \hat{T} S_j^+(\tau) S_i^-(0) \right\rangle = \frac{1}{4} \left\langle \hat{T} b_{j,\uparrow}^\dagger(\tau) b_{j,\downarrow}(\tau) b_{i,\downarrow}^\dagger(0) b_{i,\uparrow}(0) \right\rangle_0 \\ &= \frac{1}{4} [G_{*\uparrow\uparrow}(r, \tau) G_{\downarrow\downarrow}(r, \tau) + F_{*\uparrow\downarrow}(r, \tau) F_{\downarrow\uparrow}(r, \tau)], \end{aligned} \quad (\text{S55})$$

with the corresponding form in momentum and frequency space

$$\begin{aligned} \chi^{+-}(\mathbf{k}, i\omega_n) &= \int_0^\beta d\tau \sum_i e^{-ik \cdot r} e^{i\omega_n \tau} \chi^{+-}(r, \tau) \\ &= -\frac{1}{N} \frac{1}{16} \sum_q \frac{\left(E_q^b E_{-k-q}^b - \lambda_q \lambda_{-k-q} \right) + i\omega_n \left(-E_{-k-q}^b \lambda_q + E_q^b \lambda_{-k-q} \right) / \left(E_q^b + E_{-k-q}^b \right) + \Delta_q \Delta_{-k-q}}{E_q^b E_{-k-q}^b} \\ &\quad \times \left(-\frac{1}{i\omega_n - E_q^b - E_{-k-q}^b} + \frac{1}{i\omega_n + E_q^b + E_{-k-q}^b} \right). \end{aligned} \quad (\text{S56})$$

As a result, the imaginary part of the dynamic spin susceptibility Eqs. (S56) and (S54), after the analytic continuation $i\omega_n \rightarrow \omega + i\Gamma$, is depicted in Figs. 4(c) and (d).

V. Numerical details and additional simulation results

In this section, we offer technical information on the density matrix renormalization group (DMRG) simulations mentioned in the main text and additional numerical results to support our conclusions further.

A. Numerical details

Extensive DMRG studies in the past few years of the Fermi-Hubbard and fermionic t - J models have accumulated valuable experience and techniques on how to determine the ground-state properties of 2D systems [17–27], providing helpful guidance for our current DMRG simulations of the bosonic t - J model. We implement two DMRG schemes independently to obtain reliable results.

- Grand canonical ensemble (GCE) calculations where spontaneous $U(1)$ symmetry breaking is allowed giving rise to non-zero order parameters of pairing or single-particle condensation [26, 27]. A chemical potential term $H_\mu = -\mu \sum_i n_i$ is introduced to control the doping level δ indirectly. The bond dimensions are kept up to $D = 4000$ in the GCE simulations only to measure local properties on the natural ground states [27] within broken symmetry plateaus [26]. This scheme can be considered as a certain interpolation between the exact ground states and the mean-field solutions, where the local properties can faithfully reflect the tendencies of long-range orders in the true ground state, despite that the long-distance correlations obtained by this scheme may not be accurate. We perform a variety of simulations with different initial states and temporary pinning fields to avoid being stuck in metastable states. The spin- $U(1)$ symmetry is imposed in some of the GCE simulations in the AFM-PDW phase to speed up the computations and control the spin-rotation symmetry-breaking axis.

- Canonical ensemble (CE) calculations where the charge- $U(1)$ and spin- $U(1)$ symmetries are imposed to fix the total particle number (hence the doping level) and total spin S^z . The phases of matter are determined by computing the decay behaviors of long-distance correlation functions [17–25]. The bond dimensions are kept up to $D = 16000$ in the CE simulations to obtain accurate results with truncation error $\epsilon \lesssim 5 \times 10^{-6}$.

Our primary focus is the GCE simulations for width-8 systems and the CE simulations for width-4 systems, which yield consistent phase diagrams. Other scenarios like width-2 and width-6 systems are also simulated in certain cases to support our conclusions further. We exploit either cylindrical boundary conditions (periodic in the \hat{y} direction and open in the \hat{x} direction) like the 32×8 cylinder in or fully open boundary conditions (open in both the \hat{x} and \hat{y} directions).

In particular, we remark that though spontaneous symmetry breaking can automatically occur in the GCE simulations even without any external pinning fields (which is checked by our simulations), sometimes we still apply very small pinning fields (around 10^{-2}) on the lattice edges at the initial stage of DMRG optimization (when the bond dimension is relatively small) to induce symmetry breaking and stabilize the symmetry-breaking directions, such as the PDW pinning field $H_{\text{PDW}} = -h_{\text{PDW}} \sum_{i\alpha} (-1)^{x+y} (\Delta_{i\alpha} + \Delta_{i\alpha}^\dagger)$ with $i = (x, y)$, the AFM pinning field $H_{\text{AFM}} = -h_{\text{AFM}} \sum_i (-1)^{x+y} S_i^z$, the SF pinning field $H_{\text{SF}} = -h_{\text{SF}} \sum_{i\sigma} (B_{i\sigma} + B_{i\sigma}^\dagger)$, and the FM pinning field $H_{\text{FM}} = -h_{\text{FM}} \sum_i S_i^z$. The pinning fields are removed after a few sweeps and no pinning field is applied at the end of optimization. Combined with the consistent results from the CE calculations, one can reliably obtain the general phase diagram relevant to the 2D bosonic t - J model.

In addition, we use the notation $\langle \Delta_{i\alpha} \rangle$ and $\langle B_{i\sigma} \rangle$ to denote the pairing and single-boson condensation local order parameters in the main text, which are real numbers in the numerical results. In principle, there is a phase arbitrariness for these $U(1)$ symmetry-breaking order parameters. Here we fix this arbitrariness or say ‘‘symmetry-breaking axis’’ by code implementation with real-number wavefunctions such that $\langle \Delta_{i\alpha} \rangle$ and $\langle B_{i\sigma} \rangle$ are always real numbers. This implementation can also speed up the computations and improve the stability of the numerical results across different model parameters. Thus, the values of $\langle \Delta_{i\alpha} \rangle$ and $\langle B_{i\sigma} \rangle$ in the main text should be understood as the magnitudes along the symmetry-breaking axis.

B. Additional simulation results

1. Correlation function analysis for the bosonic t - J model

We first provide a detailed analysis of the correlation function data from the CE calculations for width-4 systems. Fig. S4 shows the correlation functions in the ground state of the bosonic t - J model on cylinders of size 32×4 for the doping levels $\delta = 0, 1/64, 1/32, 1/16, 1/8, 1/4, 1/2$ and size 36×4 for the doping levels $\delta = 1/6, 1/3$. The spin-singlet pair-pair correlation is defined as

$$P_{\alpha\beta}(r) = \langle \Delta_{i_0\alpha}^\dagger \Delta_{(i_0+r),\beta} \rangle, \quad (\text{S57})$$

where $\Delta_{i\alpha} = \frac{1}{\sqrt{2}} \sum_{\sigma} \sigma B_{i,\sigma} B_{i+\alpha,-\sigma}$ is the spin-singlet pair annihilation operator. $\alpha \in \{\hat{x}, \hat{y}\}$ denotes the nearest-neighbor (NN) link. \hat{x} and \hat{y} denotes the two unit basis vectors of the square lattice. σ takes $\{+1, -1\}$ for $\{\uparrow, \downarrow\}$ when serving as a coefficient. $i_0 = (x_0, y_0)$ is the reference site and r is a real space vector connecting the created and annihilated particles. By default, we take $x_0 = L_x/4$ and set the distance vector r along the \hat{x} -direction. The spin-spin correlation is defined as

$$F_{\gamma}(r) = \langle S_{i_0}^{\gamma} S_{i_0+r}^{\gamma} \rangle, \quad (\text{S58})$$

where $\gamma \in \{x, y, z\}$ denotes the spin component. The single-particle Green’s function and the density-density correlation are defined as

$$G_{\sigma}(r) = \langle B_{i_0,\sigma}^\dagger B_{(i_0+r),\sigma} \rangle, \quad (\text{S59})$$

$$D(r) = \langle n_{i_0} n_{i_0+r} \rangle - \langle n_{i_0} \rangle \langle n_{i_0+r} \rangle. \quad (\text{S60})$$

The density average $\langle n_i \rangle$ is subtracted in $D(r)$ to represent the correlation of density fluctuations. We summarize the corresponding extracted power exponent K and correlation length ξ by fitting the power-law decay $\sim r^{-K}$ and the exponential decay $\sim e^{-r/\xi}$ respectively in Table. S1.

Intermediate region.—Besides the prominent AFM-PDW and FM-SF phases discussed in the main text, Fig. S4 reveals an intermediate transition region between the two phases, including $\delta = 1/6, 1/4$ at least in the level of

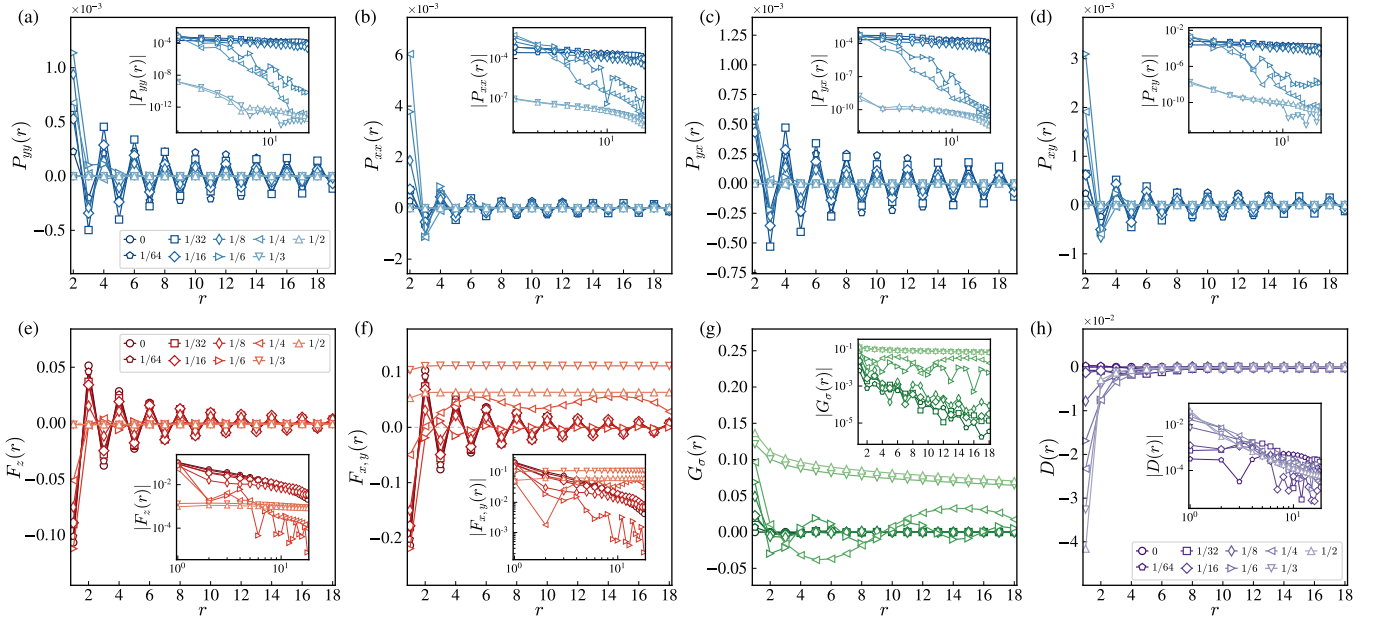


FIG. S4. Correlation functions in the ground state of the bosonic t - J model on cylinders of size 32×4 or 36×4 with $t/J = 3$ and varying doping level δ labeled by different markers. (a-d) Spin-singlet pair-pair correlation between two NN links oriented in the $\{\hat{x}, \hat{y}\}$ directions. (e,f) Spin-spin correlation along the S^z and $S^{x,y}$ directions. (g) Single-particle Green's function. (h) Density-density correlation. The inset shows the logarithmic or semi-logarithmic plots.

Phase	Doping	$G_\sigma(r)$	$P_{\alpha\beta}(r)$	$F_z(r)$	$F_{xy}(r)$	$D(r)$
AFM*	$\delta = 0$	$= 0$	$= 0$	$K_F \approx 1.3, \xi_F \approx 5$	$K_F \approx 1.3, \xi_F \approx 5$	$= 0$
AFM + π -PDW	$\delta = 1/32$	$\xi_G \approx 3$	$K_P \approx 0.8$	$K_F \approx 1.1$	$K_F \approx 1.1$	$K_D \approx 2$
	$\delta = 1/16$	$\xi_G \approx 3$	$K_P \approx 1.0$	$K_F \approx 0.9$	$K_F \approx 0.9$	$K_D \approx 2$
	$\delta = 1/8$	$\xi_G \approx 3$	$K_P \approx 1.0$	$K_F \approx 0.9$	$K_F \approx 0.9$	$K_D \approx 2$
Transition region	$\delta = 1/6$	$K_G \approx 0.6$	$\xi_P \approx 1$	$K_F \approx 1.8, \xi_F \approx 4$	$K_F \approx 0.7$	$K_D \approx 2$
	$\delta = 1/4$	$K_G \approx 0.2$	$\xi_P \approx 1$	$K_F \approx 1.8, \xi_F \approx 4$	$K_F \approx 0$	$K_D \approx 2$
FM + SF	$\delta = 1/3$	$K_G \approx 0.2$	≈ 0	$\approx 10^{-3}$	$\approx 10^{-1}$	$K_D \approx 2$
	$\delta = 1/2$	$K_G \approx 0.2$	≈ 0	$\approx 10^{-3}$	$\approx 10^{-1}$	$K_D \approx 2$

TABLE S1. The estimated fitting exponents for the correlation functions in the ground states of the bosonic t - J model at $t/J = 3$ on 4-leg cylinders. The system size is chosen as 32×4 for $\delta = 0, 1/32, 1/16, 1/8, 1/4, 1/2$ and 36×4 for $\delta = 1/6, 1/3$. $G_\sigma(r)$, $P_{\alpha\beta}(r)$, $F_z(r)$, $F_{xy}(r)$ and $D(r)$ represent the single-particle Green's function, singlet pair-pair correlation, spin-spin correlation along z and x, y direction, and density-density correlation. The singlet pair orientation in $P_{\alpha\beta}(r)$ takes values in $\alpha, \beta \in \{\hat{x}, \hat{y}\}$, the information of which are merged into one column as they have similar decaying behaviors. The spin orientation in $G_\sigma(r)$ takes values in $\sigma \in \{\uparrow, \downarrow\}$, which are also merged into one column as they have the same decaying behaviors. The notations K_G , K_P , and K_F stand for power-law fitting r^{-K} while ξ_G , ξ_P , ξ_F and ξ_D stands for exponential fitting $e^{-r/\xi}$. The cases where two fitting exponents are both shown mean that considerable ambiguity exists in determining fitting schemes due to numerical uncertainty. Here "AFM*" means that though a spin gap is observed due to the finite-size effects of even-leg ladders, a true AFM long-range order will be developed in the 2D limit.

$L_y = 4$, where the correlation functions strongly fluctuate without a clear pattern that can be easily identified. This intermediate region also shows signatures in the simulations for systems of $L_y = 8$, where the doping level δ can hardly fall into the interval near $\delta_c \approx 0.2$ by tuning the chemical potential μ , suggesting that it is an unstable region with relatively high entanglement that is hard to be captured by DMRG simulations, compared to the stable phases on both sides. Thus, we consider the region as a transition region instead of a new well-defined phase, as indicated by the grey area in Fig. 1(a). In the 2D thermodynamic limit, this transition region could either shrink into a true quantum critical point or persist as a finite region, a question we leave for future research.

Spin gap in half-filled finite-width systems.—For narrow ladders with even legs such as the width-4 systems investigated here, it is believed that a spin gap exists at half-filling based on numerical experience and the argument that an

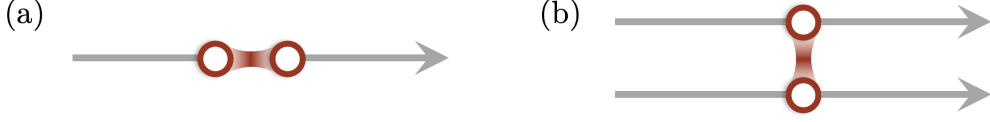


FIG. S5. Illustration of two different modes of hole pair motion: (a) “in-tandem” vs (b) “side-by-side”. The moving direction is always parallel to the bond direction of the hole pair in (a) while perpendicular to the bond direction in (b).

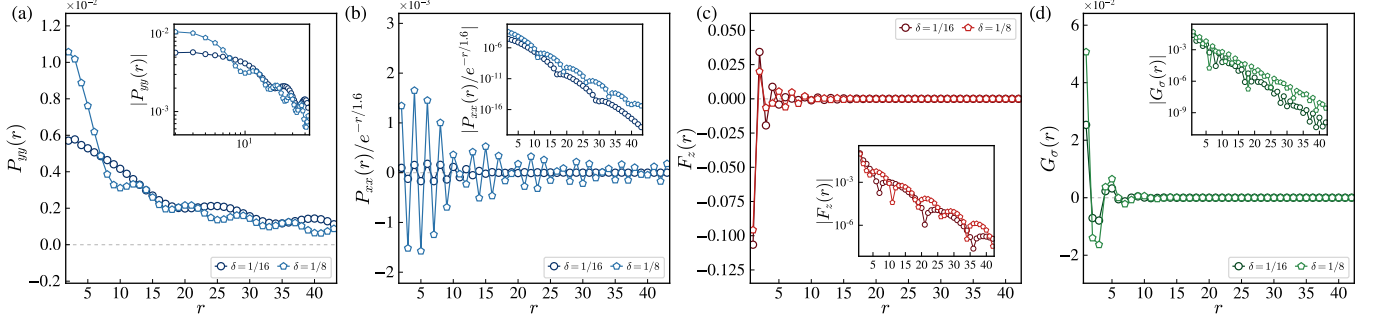


FIG. S6. Correlation functions in the ground state of the bosonic t - J model on 2-leg ladders of size 64×4 with $t_y = 0$, $t_x/J = 3$ and varying doping level δ . (a,b) Spin-singlet pair-pair correlation between two NN links oriented in the $\{\hat{x}, \hat{y}\}$ directions. The correlation function in (b) is rescaled and divided by a factor $e^{-r/1.6}$ to show the oscillation pattern more clearly. (c) Spin-spin correlation along the S^z direction. (d) Single-particle Green’s function. The inset shows the logarithmic or semi-logarithmic plots.

even number of $S = 1/2$ spins on a rung constitutes an integer spin, and the resulting integer spin chain is gapped in a similar spirit of Haldane’s conjecture. This is indeed observed by our simulations for width-4 systems as shown by the spin-spin correlations at $\delta = 0$ in Fig. S4 and Table. S1. However, the spin gap, as a finite-width effect, will vanish in the 2D limit where a true long-range AFM order develops, as suggested by the spontaneous AFM patterns observed in our GCE simulations for width-8 systems. Upon doping, the AFM spin-spin correlation in the CE calculations is enhanced counter-intuitively to a quasi-long-range behavior. The spontaneous AFM order parameter in the GCE calculations is also enhanced upon doping, as shown in Fig. 1(d). This can be understood by the fact that, in the low doping regime, the doped holes form tightly bound pairs propagating “in tandem”, which respects the AFM spin background. As a result, the AFM order is not only undisturbed by the doped holes but can even be strengthened by the compatible (π, π) -PDW order.

Details on the pair-pair correlations.—The PDW immediately emerges once doping holes, as shown in Fig. S4 by the pair-pair correlation in the system with only two doped holes, i.e., of size 32×4 and doping $\delta = 1/64$. The PDW oscillation is also observed in our CE calculations for width-6 systems, albeit only in short-distance pair-pair correlations at the level of the bond dimension $D \leq 10000$ because the increased computational difficulty of width-6 systems makes it challenging to accurately calculate long-distance correlations. In the FM-SF phase, the singlet pair-pair correlations almost vanish (around 10^{-9}), as shown in Table. S1 and the insets of Fig. S4. The spin-triplet pair-pair correlations exhibit algebraic decay (not shown here), which yet does not signify true pairing but rather a secondary effect resulting from single-boson condensation.

2. Probing the phase of pairing

In the main text, we argue that the PDW results from the Marshall sign given that the fluctuating phases from imaginary time evolution under the Marshall basis are fully canceled by paired holes moving “in tandem”, as depicted in Fig. S5(a). This argument can be further justified by measuring the pair-pair correlations in the absence of the inter-leg hopping t_y (the hopping integral along the \hat{y} direction). If we set $t_y = 0$ while keeping $t_x/J = 3$, the hole pair across different legs cannot move in tandem but can only move in two separate legs respectively since the hole cannot hop among different legs. On the other hand, the hole pair within the same leg can still move in tandem. According to the argument in the main text, the former should have no PDW oscillation because an additional staggered sign arises from the “side-by-side” hopping process, as depicted in Fig. S5(b), while the latter should still have the same

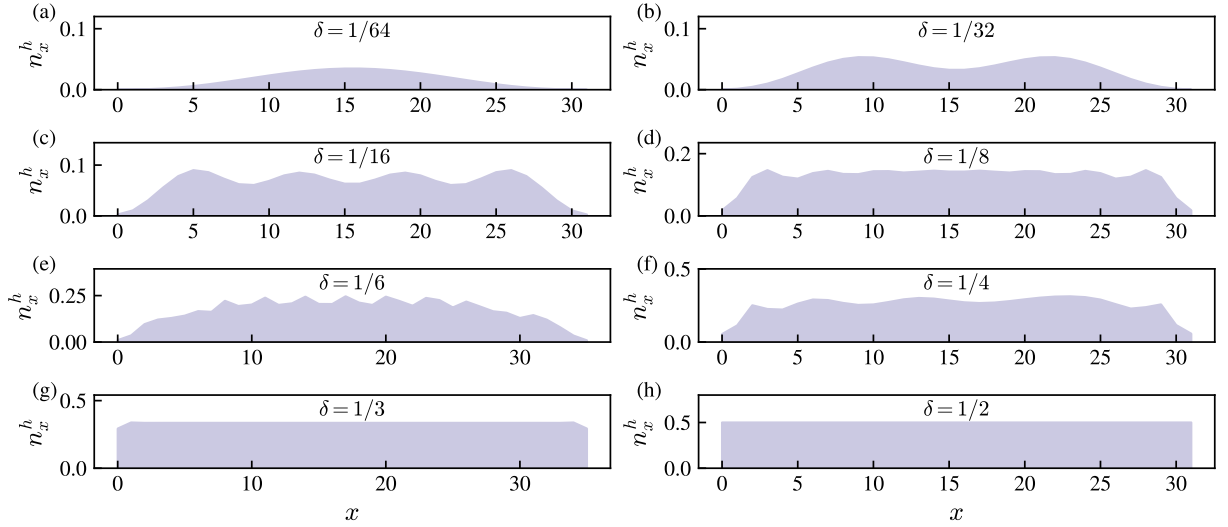


FIG. S7. The hole density profiles in the ground state of the bosonic t - J model on cylinders of size 32×4 or 36×4 with $t/J = 3$ and varying doping level δ .

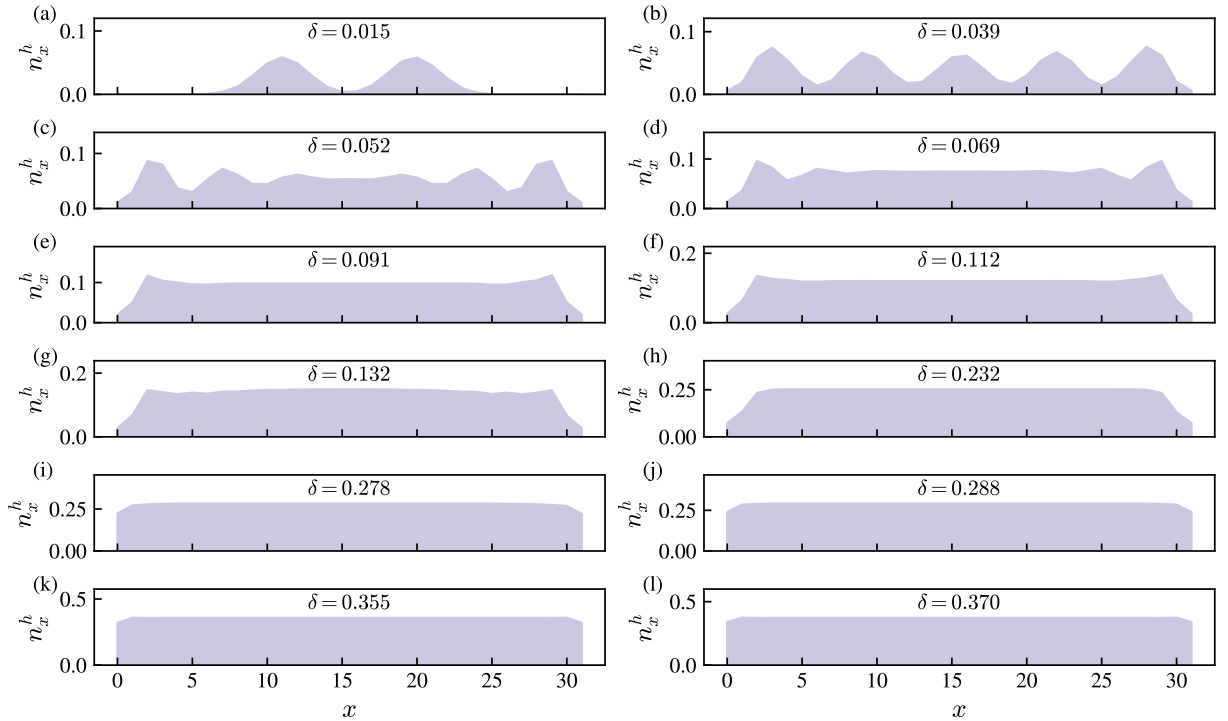


FIG. S8. The hole density profiles in the ground state of the bosonic t - J model on cylinders of size 32×8 with $t/J = 3$ and varying doping level δ .

PDW oscillation as the cases with $t_y = t_x = 3J$. Indeed, as shown by the DMRG results of 2-leg systems with $t_y = 0$ in Fig. S6, the pair-pair correlation $P_{yy}(r)$, corresponding to the hole pair across different legs, has no PDW oscillation and turns out to be positive-definite. The pair-pair correlation $P_{xx}(r)$, corresponding to the hole pair within the same leg, still has a PDW oscillation at momentum π , though it decays exponentially as the physical nature of the ground states has also been changed by enforcing the 1D hopping restriction $t_y = 0$ [60, 65]. Similar results have also been observed in width-4 systems with $t_y = 0$.

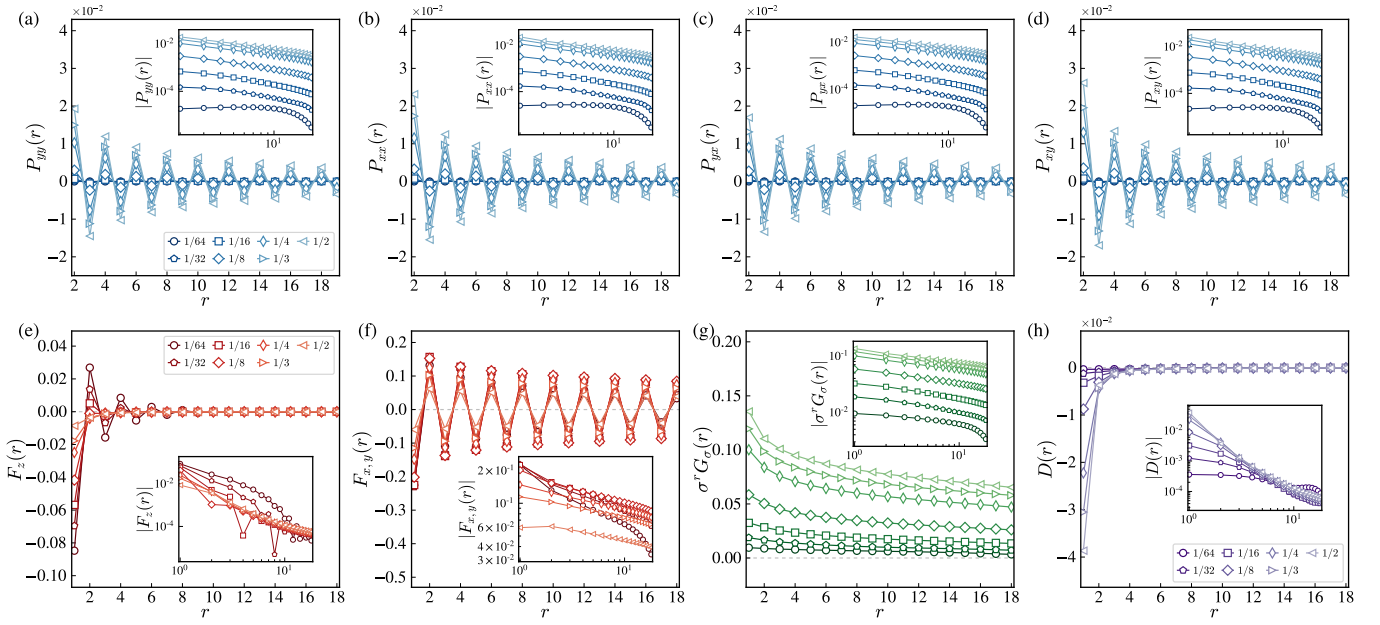


FIG. S9. Correlation functions in the ground state of the bosonic σt - J model on cylinders of size 32×4 or 36×4 with $t/J = 3$ and varying doping level δ labeled by different markers. (a-d) Spin-singlet pair-pair correlation between two NN links oriented in the $\{\hat{x}, \hat{y}\}$ directions. (e,f) Spin-spin correlation along the S^z and $S^{x,y}$ directions. (g) Single-particle Green's function. (h) Density-density correlation. The inset shows the logarithmic plots. The distinct behavior of $\delta = 1/64$ is inclined to be a finite-size effect since there are only two holes in this 32×4 system at doping $\delta = 1/64$.

3. Density distributions

Figs. S7 and S8 show the hole density profiles $n_x^h = \sum_y n_{x,y}^h / L_y$ in width-4 and width-8 systems, where $n_{x,y}^h = n_i^h = 1 - n_i$. In the FM-SF phase, the density profiles are perfectly uniform. In the AFM-PDW phase, the profiles are almost uniform in the bulk at moderately low doping $\delta \gtrsim 0.05$, but exhibit some oscillations at very low doping $\delta \lesssim 0.05$, with each peak corresponding to around 2 holes, which bears a certain resemblance with the inhomogeneity phenomena in real experiments. However, these density oscillations are different from the stripe orders commonly observed in the fermionic t - J or Hubbard models because (i) the doping levels here are extremely low compared to the fermionic case; (ii) there is no AFM domain wall across the hole density profile peaks, i.e., the AFM order persists to the entire PDW phase instead of being modulated to spin density waves (SDW) at some momentum deviating from π [29]. Moreover, the density-density correlation $D(r)$, as shown in Fig. S4 and Table. S1, decays much faster than those dominant correlations $P_{\alpha\beta}(r)$ or $G_\sigma(r)$. This feature also differs from the stripe orders in the fermionic case where the density-density correlations are dominant. From another perspective, this also suggests that the bosonic t - J model might be computationally easier than the fermionic t - J or Hubbard models due to the absence of intensely competing orders.

4. Correlation function analysis for the bosonic σt - J model

Here we provide a detailed analysis of the correlation function data from the CE calculations for the bosonic σt - J model on width-4 systems. Fig. S4 shows the correlation functions in the ground state of the bosonic t - J model on cylinders of size 32×4 for the doping levels $\delta = 1/64, 1/32, 1/16, 1/8, 1/4, 1/2$ and size 36×4 for the doping levels $\delta = 1/3$. We summarize the corresponding extracted power exponent K and correlation length ξ in Table. S2. Since this bosonic σt - J model is a sign-problem-free model, previous work has actually already performed accurate quantum Monte Carlo (QMC) calculations [68–71] on the model in Eq. (S13) which is equivalent to this bosonic σt - J model. The conclusions there are consistent with ours, also indicating an SF ground state. One benefit from repeating the simulations with DMRG here is that, the comparison with the QMC results allows us to validate the reliability of our DMRG simulations and our interpretation of the DMRG data throughout the paper, such as the extremely slow decay of $G_\sigma(r)$ in the CE calculations indeed indicates an SF phase.

Phase	Doping	$G_\sigma(r)$	$P_{\alpha\beta}(r)$	$F_z(r)$	$F_{xy}(r)$	$D(r)$
AFM*	$\delta = 0$	$= 0$	$= 0$	$K_F \approx 1.3, \xi_F \approx 5$	$K_F \approx 1.3, \xi_F \approx 5$	$= 0$
xy-AFM + SF	$\delta = 1/32$	$K_G \approx 0.3$	$K_P \approx 1$	$K_F \approx 2$	$K_F \approx 0.3$	$K_D \approx 2$
	$\delta = 1/16$	$K_G \approx 0.3$	$K_P \approx 1$	$K_F \approx 2$	$K_F \approx 0.3$	$K_D \approx 2$
	$\delta = 1/8$	$K_G \approx 0.3$	$K_P \approx 0.9$	$K_F \approx 2$	$K_F \approx 0.3$	$K_D \approx 2$
	$\delta = 1/4$	$K_G \approx 0.2$	$K_P \approx 0.8$	$K_F \approx 2$	$K_F \approx 0.2$	$K_D \approx 2$
	$\delta = 1/3$	$K_G \approx 0.2$	$K_P \approx 0.7$	$K_F \approx 2$	$K_F \approx 0.2$	$K_D \approx 2$
	$\delta = 1/2$	$K_G \approx 0.2$	$K_P \approx 0.7$	$K_F \approx 2$	$K_F \approx 0.2$	$K_D \approx 2$

TABLE S2. The estimated fitting exponents for the correlation functions in the ground states of the bosonic σt - J model at $t/J = 3$ on 4-leg cylinders. The system size is chosen as 32×4 for $\delta = 0, 1/32, 1/16, 1/8, 1/4, 1/2$ and 36×4 for $\delta = 1/3$. $G_\sigma(r)$, $P_{\alpha\beta}(r)$, $F_z(r)$, $F_{xy}(r)$ and $D(r)$ represent the single-particle Green's function, singlet pair-pair correlation, spin-spin correlation along z and x, y direction, and density-density correlation. The singlet pair orientation in $P_{\alpha\beta}(r)$ takes values in $\alpha, \beta \in \{\hat{x}, \hat{y}\}$, the information of which are merged into one column as they have similar decaying behaviors. The spin orientation in $G_\sigma(r)$ takes values in $\sigma \in \{\uparrow, \downarrow\}$, which are also merged into one column as they have the same decaying behaviors. The notations K_G , K_P and K_F stand for power-law fitting r^{-K} while ξ_G , ξ_P , ξ_F and ξ_D stands for exponential fitting $e^{-r/\xi}$. The cases where two fitting exponents are both shown mean that considerable ambiguity exists in determining fitting schemes due to numerical uncertainty. Here "AFM*" means that though a spin gap is observed due to the finite-size effects of even-leg ladders, a true AFM long-range order will be developed in the 2D limit.

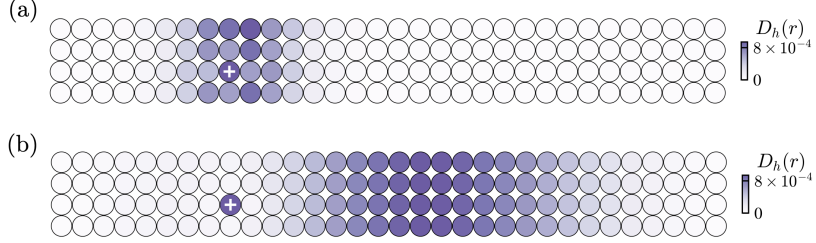


FIG. S10. The hole-hole density correlation for the two-hole-doped (a) bosonic t - J and (b) σt - J models with $t/J = 3$ on cylinders of size 32×4 . The cross represents the reference site.

5. Hole-hole correlation in two-hole-doped systems

The hole-hole density correlation is defined as $D_h(r) = \langle n_{i_0}^h n_{i_0+r}^h \rangle$. For a two-hole-doped system, $D_h(r)$ can be interpreted as the spatial distribution of one hole over the lattice given another hole is pinned at site i_0 . Hence $D_h(r)$ can be used to detect the existence of BEC-type pairing besides the pair-pair correlations. In the main text, we have shown the hole-hole correlation in width-6 systems, where the fully open boundary condition is exploited, in contrast to Ref. [56]. Fig. S10 shows the hole-hole correlation in width-4 cylinders, which yields consistent results with width-6 calculations. Namely, the two holes are very close to each other in space forming a tightly bound pair in the bosonic t - J model while exhibiting a mutually separated and loose distribution in the bosonic σt - J model, which aligns with the corresponding PDW order and SF order at the low doping regime respectively. We further plot the profile of $D_h(r)$ with r along the \hat{x} direction in Fig. S11 and extract the correlation length of $D_h(r)$ for the bosonic t - J model, which equals about one lattice constant for both width-4 and width-6 systems, implying an extremely small hole pair size in the AFM-PDW phase.

C. Measuring pair-pair correlations in cold atom simulations

To measure the correlators that are not products of Hermitian operators on quantum devices, e.g., the pair-pair correlators shown above, one needs to rewrite them as linear combinations of products of Hermitian operators. For qutrit systems where the bosonic t - J model is defined, the Pauli matrices that are used in qubit systems as an orthogonal basis should be generalized, e.g., to the Gell-Mann matrices that span the Lie algebra of the $SU(3)$ group.

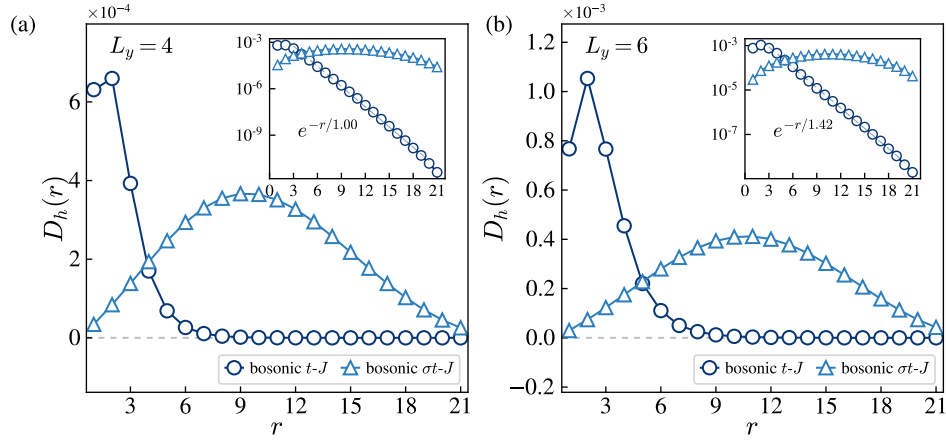


FIG. S11. The profile of the hole-hole density correlation for the two-hole-doped bosonic t - J and σt - J models with $t/J = 3$ on cylinders of size 32×4 and open square lattices of size 32×6 .

Here we exploit a more symmetric form by recombining the normal Gell-Mann matrices, i.e.,

$$\begin{aligned}
 \Lambda_{\uparrow\downarrow}^x &= |\uparrow\rangle\langle\downarrow| + |\downarrow\rangle\langle\uparrow|, & \Lambda_{\uparrow\downarrow}^y &= -i|\uparrow\rangle\langle\downarrow| + i|\downarrow\rangle\langle\uparrow|, & \Lambda_{\uparrow\downarrow}^z &= |\uparrow\rangle\langle\uparrow| - |\downarrow\rangle\langle\downarrow|, \\
 \Lambda_{\uparrow h}^x &= |\uparrow\rangle\langle h| + |h\rangle\langle\uparrow|, & \Lambda_{\uparrow h}^y &= -i|\uparrow\rangle\langle h| + i|h\rangle\langle\uparrow|, & \Lambda_{\uparrow h}^z &= |\uparrow\rangle\langle\uparrow| - |h\rangle\langle h|, \\
 \Lambda_{\downarrow h}^x &= |\downarrow\rangle\langle h| + |h\rangle\langle\downarrow|, & \Lambda_{\downarrow h}^y &= -i|\downarrow\rangle\langle h| + i|h\rangle\langle\downarrow|, & \Lambda_{\downarrow h}^z &= |\downarrow\rangle\langle\downarrow| - |h\rangle\langle h|.
 \end{aligned} \tag{S61}$$

Note that each of them is Hermitian and the three Λ^z matrices are not independent of each other, e.g., $\Lambda_{\uparrow\downarrow}^z = \Lambda_{\uparrow h}^z - \Lambda_{\downarrow h}^z$. That is to say, there are eight independent matrices, consistent with the degrees of freedom in a 3×3 unitary with determinant 1. Using the Λ matrices in Eq. (S61), the creation and annihilation operators of the hard-core bosons in the bosonic t - J model can be expressed by

$$B_\sigma = \frac{\Lambda_{\sigma h}^x - i\Lambda_{\sigma h}^y}{2}, \quad B_\sigma^\dagger = \frac{\Lambda_{\sigma h}^x + i\Lambda_{\sigma h}^y}{2}, \tag{S62}$$

where we omit the site indices for simplicity. Thus, by substituting Eq. (S62) into each creation and annihilation operator within a certain correlator, one can express any correlator as a linear combination of products of Λ matrices. We remark that the correlators defined by the products of the Λ matrices can be directly measured on quantum devices with single-qutrit rotation gates by rotating the measurement basis onto the eigenbasis of the operator to be measured. Alternatively, one can also apply randomized measurement schemes like the classical shadow tomography first and leave all the classical post-processing after measurements, which can further improve the efficiency when measuring multiple observables.